

The Key to State Reduction in Linear Attention: A Rank-based Perspective

Philipp Nazari^{1 2 3} T. Konstantin Rusch^{1 3 4 5}

Abstract

Linear attention offers a computationally efficient yet expressive alternative to softmax attention. However, recent empirical results indicate that the state of trained linear attention models often exhibits a low-rank structure, suggesting that these models underexploit their capacity in practice. To illuminate this phenomenon, we provide a theoretical analysis of the role of rank in linear attention, revealing that low effective rank can affect retrieval error by amplifying query noise. In addition to these theoretical insights, we conjecture that the low-rank states can be substantially reduced post-training with only minimal performance degradation, yielding faster and more memory-efficient models. To this end, we propose a novel hardware-aware approach that structurally prunes key and query matrices, reducing the state size while retaining compatibility with existing CUDA kernels. We adapt several existing pruning strategies to fit our framework and, building on our theoretical analysis, propose a novel structured pruning method based on a rank-revealing QR decomposition. Our empirical results, evaluated across models of varying sizes and on various downstream tasks, demonstrate the effectiveness of our state reduction framework. We highlight that our framework enables the removal of 50% of the query and key channels at only a marginal increase in perplexity. The code for this project can be found at <https://github.com/camail-official/LinearAttentionPruning>.

1. Introduction

Linear Attention (Katharopoulos et al., 2020; Schlag et al., 2021; Sun et al., 2023b; Peng et al., 2023; Gu & Dao, 2024;

¹Max Planck Institute for Intelligent Systems, Tübingen, Germany ²Department of Computer Science, ETH Zürich, Zürich, Switzerland ³ELLIS Institute Tübingen ⁴Tübingen AI Center ⁵Liquid AI. Correspondence to: Philipp Nazari <philipp.nazari@tuebingen.mpg.de>.

Preprint. February 5, 2026.

Yang et al., 2024b; Dao & Gu, 2024; Yang et al., 2024a; Team et al., 2025) has emerged as an efficient alternative to softmax attention (Vaswani et al., 2017), enabling high-throughput chunkwise parallel training (Hua et al., 2022; Sun et al., 2023b; Lingle, 2023; Yang et al., 2023) with linear time complexity and constant memory inference. These efficiency gains have recently driven the development of large hybrid models (Lieber et al., 2024; Li et al., 2025; Blakeman et al., 2025; Team, 2025) which predominantly employ linear attention layers, interspersed with only a few softmax attention layers.

Despite their impressive performance, prior work indicates that linear attention models still underutilize their capacity in practice (Siems et al., 2025; Parnichkun et al., 2025). In particular, the matrix-valued hidden states that implement the associative memory exhibit a low-rank structure after training. As we show, this structure can increase the model’s sensitivity to query noise. This finding suggests that the state size can be reduced post-training, yielding models that are both faster and more memory-efficient.

Towards this end, we propose a novel structured pruning framework to reduce the size of the hidden states in linear attention models. Within this framework, our experiments reveal that we can consistently remove approximately 50% of the key and query channels at only a minor increase in perplexity, even before recovery fine-tuning. Unlike methods like SliceGPT (Ashkboos et al., 2024a), SpinQuant (Liu et al., 2024) and QuaRot (Ashkboos et al., 2024b), which introduce rotations in the *embedding space*, our framework operates in the *state space*. Our framework is thus complementary to these methods.

Specifically, our approach relies on the observation that linear attention models are invariant under orthogonal transformations applied jointly to the queries and keys. Building on this insight, we seek transformations that select the columns of the keys and queries that contribute substantially to model performance. Within this framework, we reformulate several existing pruning strategies, including magnitude-based and gradient-saliency-based ones. Motivated by theoretical insights, we furthermore introduce a novel structured pruning approach that selects a subset of columns that maximizes the rank utilization of the remaining memory.

In summary, our **main contributions** are:

- We provide theoretical insights into the role of rank in linear attention (Section 2.1). We show that rank utilization, a measure of memory isotropy, directly affects retrieval error, and that low rank utilization can amplify query noise.
- Motivated by the low rank utilization observed in practice, we formulate a novel post-training state-size reduction framework (Section 3). Specifically, we show that the state can be reduced substantially by jointly selecting subsets of channels from the keys and queries.
- We adapt several existing pruning strategies to fit our framework and, building on our theoretical analysis, propose a novel structured pruning method based on rank-revealing QR decompositions (Section 3.3).
- We present extensive empirical results on multiple large, pretrained linear attention models evaluated across a range of zero-shot and recall tasks, demonstrating the effectiveness of our proposed framework (Section 5.1).

2. Theoretical Insights

In this section, we first introduce linear attention and describe the role of the hidden state as an associative memory, before developing a framework to assess how effectively it is utilized.

2.1. Background on Linear Attention

Softmax attention maps an input sequence $\mathbf{X} \in \mathbb{R}^{T,h}$ to queries $\mathbf{Q} = \mathbf{X}\mathbf{W}_Q \in \mathbb{R}^{T,d_k}$, keys $\mathbf{K} = \mathbf{X}\mathbf{W}_K \in \mathbb{R}^{T,d_k}$, and values $\mathbf{V} = \mathbf{X}\mathbf{W}_V \in \mathbb{R}^{T,d_v}$ via linear projections. The output of the attention layer can then be computed in parallel,

$$\mathbf{O} = \text{softmax} \left(\frac{\mathbf{Q}\mathbf{K}^\top}{\sqrt{d_k}} \right) \mathbf{V} \in \mathbb{R}^{T,d_v}. \quad (1)$$

Equivalently, the same operation can be expressed sequentially: for each time step t ,

$$\mathbf{o}_t = \sum_{s=1}^t \frac{\exp(\mathbf{q}_t \mathbf{k}_s^\top / \sqrt{d_k})}{\sum_{j=1}^t \exp(\mathbf{q}_t \mathbf{k}_j^\top / \sqrt{d_k})} \mathbf{v}_s \in \mathbb{R}^{d_v}. \quad (2)$$

The parallel formulation is commonly used during training and takes advantage of GPU parallelism; however, it imposes quadratic time and memory complexity. The sequential formulation is used at inference and can also be implemented as a KV-cache (Pope et al., 2023). It is worth noting that, even then, the sequential formulation still requires $O(T)$ memory, which is specifically problematic for longer sequences.

Linear attention (Schlag et al., 2021; Yang et al., 2024b; Dao & Gu, 2024; Yang et al., 2024a; Siems et al., 2025)

addresses this bottleneck by removing the softmax operator in Equation (1) and exploiting the associativity of matrix multiplication:

$$(\mathbf{Q}\mathbf{K}^\top) \mathbf{V} = \mathbf{Q} (\mathbf{K}^\top \mathbf{V}).$$

Based on this rearrangement, the softmax-free sequential version of Equation (2) can be expressed recurrently,

$$\mathbf{S}_t = \mathbf{S}_{t-1} + \mathbf{v}_t \mathbf{k}_t^\top, \quad (3)$$

where $\mathbf{S}_t \in \mathbb{R}^{d_v, d_k}$ is a matrix-valued hidden state used to compute the output $\mathbf{o}_t = \mathbf{S}_t \mathbf{q}_t$. In this work, we will refer to \mathbf{S}_t as the associative memory, and the update rule of \mathbf{S}_t as the sequence mixer.

Clearly, the mechanism defined in Equation (3) can only write *into* the associative memory \mathbf{S}_t . DeltaNet (Schlag et al., 2021; Yang et al., 2024b) addresses this limitation by explicitly erasing old information correlated with the current key before writing the new value to \mathbf{S}_t , i.e.,

$$\mathbf{S}_t = \mathbf{S}_{t-1} (\mathbf{I} - \beta_t \mathbf{k}_t \mathbf{k}_t^\top) + \beta_t \mathbf{v}_t \mathbf{k}_t^\top. \quad (4)$$

Gated DeltaNet (Yang et al., 2024a) further refines this mechanism by introducing a data-dependent decay term.

2.2. On the Role of the Rank

A commonly identified weakness of linear attention models is their fixed-sized associative memory. However, recent empirical results indicate that these models do not manage this memory well (Siems et al., 2025; Parnichkun et al., 2025) and exhibit a low-rank structure in practice. In the following, we build a framework that illuminates this phenomenon.

One can show that the row space of the associative memory of a family of linear attention models satisfies

$$\text{row } \mathbf{S}_t \subseteq \text{span} \langle \mathbf{k}_1, \dots, \mathbf{k}_t \rangle,$$

while its column space satisfies

$$\text{col } \mathbf{S}_t \subseteq \text{span} \langle \mathbf{v}_1, \dots, \mathbf{v}_t \rangle.$$

It thus follows that

$$\text{rank } \mathbf{S}_t \leq \min(\text{rank } \mathbf{K}_t, \text{rank } \mathbf{V}_t) \leq t, \quad (5)$$

where $\mathbf{K}_t = [\mathbf{k}_1, \dots, \mathbf{k}_t]$ and $\mathbf{V}_t = [\mathbf{v}_1, \dots, \mathbf{v}_t]$ are the matrices obtained by stacking the keys and values, respectively. The proof may be found in Appendix F.2.

Equation (5) shows that the algebraic rank of the associative memory is bounded by the ranks of the keys and values. However, this notion is too rigid to serve as a meaningful measure for noisy real-world data. We therefore shift our focus to the *effective rank* (or *stable rank*) (Rudelson & Vershynin, 2007; Tropp et al., 2015; Vershynin, 2018; Ipsen & Saibaba, 2025), a surrogate for the numerical rank (Vershynin, 2018, Section 2.8):

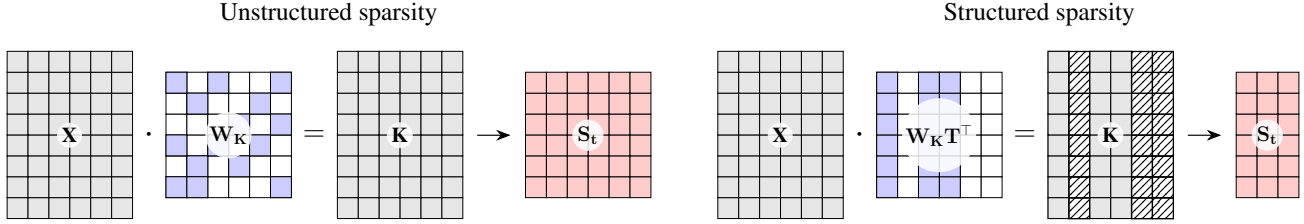


Figure 1. Left: Unstructured pruning yields a sparse weight matrix \mathbf{W}_K yet preserves the column dimension of \mathbf{K} , leaving the domain of the state matrix $\mathbf{S}_t \in \mathbb{R}^{d_v, d_k}$ invariant. **Right:** Structured pruning eliminates basis vectors, mapping keys to a lower-dimensional space $\mathbb{R}^{d'_k}$ where $d'_k < d_k$. This results in a compressed state $\mathbf{S}_t \in \mathbb{R}^{d_v, d'_k}$. This reduction strictly decreases the FLOP count required to compute the recurrence. This figure is inspired by [Ashkboos et al. \(2024a, Figure 1\)](#).

Definition 2.1 (Effective Rank [\(Ipsen & Saibaba, 2025\)](#)). For a matrix $\mathbf{A} \in \mathbb{R}^{m,n}$, we define the *effective rank* as

$$\text{sr}(\mathbf{A}) := \|\mathbf{A}\|_F^2 / \|\mathbf{A}\|_2^2.$$

The effective rank measures the skewness of the singular value spectrum and can also be computed as

$$\text{sr}(\mathbf{A}) = \frac{\sum_i \sigma_i^2}{\sigma_1^2},$$

where $\sigma_1 \geq \dots \geq \sigma_{\max(m,n)} \geq 0$ are the singular values of \mathbf{A} . It serves as a measure for how a model manages its hidden state.

The following proposition generalizes Equation (5), relating the effective rank of the associative memory to that of the keys. It serves as a first tool that provides control over the effective rank of the associative memory:

Proposition 2.2. *Consider the linear attention recurrence $\mathbf{S}_t = \mathbf{S}_{t-1} + \mathbf{v}_t \mathbf{k}_t^\top$. There exists a scalar quantity $\nu(\mathbf{V}_t)$ such that the effective rank of the memory is lower bounded:*

$$\frac{\nu(\mathbf{V}_t)}{\kappa^2(\mathbf{K}_t)} \leq \text{sr}(\mathbf{S}_t).$$

The proof of this proposition may be found in [Appendix F.1](#). Although this statement holds for the specific case for plain linear attention, we use it as an approximation for (Gated) DeltaNet. It establishes that the conditioning of the keys, $\kappa(\mathbf{K}_t)$, is tightly connected to the effective rank of the hidden state. Towards our goal of improving the memory utilization of linear attention models, this proposition shows that improving the conditioning of the keys improves the effective rank of the memory.

2.2.1. RANK UTILIZATION

While the effective rank measures the raw dimensionality of the stored information, it does not tell us how *efficiently* a model uses its available memory. We thus introduce the notion of rank utilization:

Definition 2.3 (Rank Utilization). Given a non-zero matrix $\mathbf{S} \in \mathbb{R}^{d_v, d_k}$, its *rank utilization* is the ratio of its effective rank and its theoretically maximal rank:

$$u(\mathbf{S}) := \frac{\text{sr}(\mathbf{S})}{\min(d_v, d_k)}.$$

Rank utilization combines effective rank and theoretically maximum capacity $d := \min(d_k, d_v)$ and thus serves as a measure for memory utilization. We identify the following two edge cases:

- **Low Utilization** ($u \ll 1$): The memory suffers from *rank collapse*. Its energy is concentrated in a few principal components. The vast majority of information stored in the state is redundant.
- **High Utilization** ($u \approx 1$): The memory is *isotropic*. Energy is distributed evenly across all dimensions.

The following is a corollary of [Proposition 2.2](#), relating the rank utilization of the keys to that of the memory:

Corollary 2.4. *It holds that*

$$\frac{\nu(\mathbf{V}_t)}{d \kappa^2(\mathbf{K}_t)} \leq u(\mathbf{S}_t).$$

In particular, since $u(\mathbf{K}_t) \geq \kappa^{-2}(\mathbf{K}_t)$ (see [Proposition D.5](#)), minimizing the condition number increases the rank utilization of the keys at a given maximum capacity d . We conclude that *maximizing rank utilization of the keys increases that of the memory*.

2.2.2. WHY DOES RANK UTILIZATION MATTER?

In this section, we demonstrate why high effective rank (that is, a flat spectrum of the associative memory) can be beneficial for retrieval from linear attention models.

Let $\mathbf{S} = \sum_{i=1}^d \sigma_i \mathbf{u}_i \mathbf{w}_i^\top$ be the SVD of the associative memory at a given time (we drop the subscript t here for brevity), with singular values $\sigma_1 \geq \dots \geq \sigma_d > 0$. Moreover, consider a noisy query $\tilde{\mathbf{q}} = \mathbf{q}^* + \mathbf{n}$, where \mathbf{q}^* is the pure query and \mathbf{n} is noise. To analyze how the memory structure affects the output error, define two coefficients that capture

the alignment δ of the noise and of the signal (denoted by γ) with the principal axis:

$$\delta := \frac{|\mathbf{n}^\top \mathbf{w}_1|}{\|\mathbf{n}\|_2} \quad \text{and} \quad \gamma := \frac{|\mathbf{q}^{*\top} \mathbf{w}_1|}{\|\mathbf{q}^*\|_2}.$$

The following theorem establishes that the relative retrieval error is governed by the stable rank $\text{sr}(\mathbf{S})$.

Theorem 2.5 (Effective Rank Governs Retrieval Error). *The ratio of the relative output error to the input noise-to-signal ratio is governed by the effective rank of the memory:*

$$\frac{\delta}{\sqrt{\text{sr}(\mathbf{S})}} \leq \frac{\|\mathbf{o} - \mathbf{o}^*\|_2 / \|\mathbf{o}^*\|_2}{\|\mathbf{n}\|_2 / \|\mathbf{q}^*\|_2} \leq \frac{\sqrt{\text{sr}(\mathbf{S})}}{\gamma}, \quad (6)$$

where κ denotes the l^2 condition number.

The proof may be found in Appendix F.3. Equation (6) can also be expressed in terms of rank utilization, since $u(s) = \text{sr}(\mathbf{S})/d$ for a given maximum capacity $d = \min(d_k, d_v)$. In this formulation, Theorem 2.5 reveals the influence of rank utilization on the retrieval error. We highlight two regimes:

- **Low Utilization ($u(\mathbf{S}) \ll 1$):** The system is highly sensitive to noise, unless it is orthogonal to the principal component of the memory ($\delta \approx 0$). Simultaneously, the upper bound is small only if the signal is aligned with the principal component ($\gamma \approx 1$). The rank utilization acts as a multiplier to the alignment of the noise with the principal component.
- **High Utilization ($u(\mathbf{S}) \approx 1$):** The memory becomes isotropic, all dimensions carry the same energy. Rank utilization acts only as a weak multiplier on the alignment of the noise and signal with the principal component. The model is not overly sensitive to noise along the principal component.

The following corollary builds on Theorem 2.5 and bounds the expected retrieval error:

Corollary 2.6 (Expected Error Bounds). *Assume the noise is isotropic Gaussian, $\mathbf{n} \sim \mathcal{N}(\mathbf{0}, \xi^2 \mathbf{I})$. Assume furthermore, for simplicity, that $\|\mathbf{q}^*\|_2 = 1$. Then the expected relative error is bounded by*

$$\sqrt{\frac{2}{\pi \text{sr}(\mathbf{S})}} \xi \leq \mathbb{E} \left[\frac{\|\mathbf{o} - \mathbf{o}^*\|_2}{\|\mathbf{o}^*\|_2} \right] \leq \frac{\sqrt{\text{sr}(\mathbf{S})}}{\gamma} \xi \mu,$$

where $\mu := \sqrt{2\Gamma(\frac{d+1}{2})/\Gamma(\frac{d}{2})}$.

The proof may be found in Appendix F.4. We furthermore provide a tighter bound including the condition number of \mathbf{S} instead of its rank utilization in Appendix B.3.

These results contextualize our observations on rank utilization in pre-trained linear attention models, revealing that

an ill-conditioned associative memory can effectively amplify query noise. This sheds further light on the role of the associative memory’s effective rank and provides a theoretical justification for our structured pruning framework, extending beyond raw efficiency gains. To this end, the following section develops hardware-aware pruning methods. It culminates in our proposed DRRQR algorithm, which optimizes rank utilization of the associative memory at a fixed compression ratio.

3. The Proposed Pruning Approach

In this section, we propose a structured pruning framework to reduce the per-head key dimension of linear attention models, which yields strictly smaller associative memories with higher throughput and lower memory requirements.

3.1. Invariant Transformations for Linear Attention

Decomposing \mathbf{S}_t row-wise reveals that the mixer simulates d_v parallel, independent linear time-varying (LTV) systems. Let $\mathbf{h}_t^{(i)} \in \mathbb{R}^{d_k}$ denote the transpose of the i -th row of \mathbf{S}_t . Each value channel $i \in \{1, \dots, d_v\}$ follows the vector-valued dynamics:

$$\mathbf{h}_t^{(i)} = \mathbf{A}_t^\top \mathbf{h}_{t-1}^{(i)} + \mathbf{B}_t v_{t,i},$$

where the system matrices $\mathbf{A}_t = \mathbf{I} - \beta_t \mathbf{k}_t \mathbf{k}_t^\top$ and $\mathbf{B}_t = \beta_t \mathbf{k}_t$ are shared across all value channels. The readout is computed via $\mathbf{C}_t = \mathbf{q}_t^\top$.

Using this perspective, we can derive the following proposition about the rotational invariance of DeltaNet:

Proposition 3.1 (Orthogonal Invariance of Sequence Mixing). *Let $\mathbf{T} \in O(d_k)$ be an orthogonal matrix. Then the (Gated) DeltaNet attention mechanism is invariant under the simultaneous transformation $(\mathbf{k}_t, \mathbf{q}_t) \mapsto (\mathbf{T}\mathbf{k}_t, \mathbf{T}\mathbf{q}_t)$.*

This transformation can be understood as performing a change of basis in the state space via an invertible matrix $\mathbf{T} \in \text{GL}(d_k)$, which changes the system matrices $(\mathbf{A}_t, \mathbf{B}_t, \mathbf{C}_t)$ to $(\mathbf{T}^{-\top} \mathbf{A}_t \mathbf{T}^\top, \mathbf{T}\mathbf{B}_t, \mathbf{C}_t \mathbf{T}^{-1})$. This transformation preserves the input-output map (Chen, 1984, Chapter 4.4). However, only requiring invertibility of \mathbf{T} is not enough, as the transformed state transition matrix

$$\tilde{\mathbf{A}}_t = \mathbf{T}^{-\top} \mathbf{A}_t \mathbf{T}^\top = \mathbf{I} - (\mathbf{T}^{-\top} \mathbf{k}_t)(\mathbf{T}\mathbf{k}_t)^\top,$$

is not symmetric and can thus not be expressed as a DeltaNet. However, if we restrict \mathbf{T} to be orthogonal, this basis change can be absorbed directly into the keys and queries as $\tilde{\mathbf{k}}_t = \mathbf{T}\mathbf{k}_t$ and $\tilde{\mathbf{q}}_t = \mathbf{T}\mathbf{q}_t$, preserving the structure of the DeltaNet recurrence. We thus conclude that a change of basis for DeltaNet models can be achieved by *applying orthogonal transformations to queries and keys simultaneously*.

3.2. State Size Reduction Requires Structured Pruning

Most existing pruning approaches for Large Language Models generally rely on unstructured or semi-structured sparsity (Frantar & Alistarh, 2023; Sun et al., 2023a). However, these methods do not reduce the state dimension of the dynamical system, as they leave the query and key vectors dense (see Figure 1). To address this issue, we focus on *structured* pruning.

Formally, given a *semi-orthogonal*¹ matrix $\mathbf{T} \in \mathbb{R}^{d'_k, d_k}$ with target dimension $d'_k < d_k$, we apply it *jointly* to the keys and queries before computing the dynamical system:

$$(\mathbf{k}_t, \mathbf{q}_t) \rightarrow (\mathbf{T}\mathbf{k}_t, \mathbf{T}\mathbf{q}_t) \quad \forall t = 1, \dots, T.$$

By Proposition 3.1, if $d'_k = d_k$, this transformation yields an equivalent realization of the dynamical system. Thus, our goal is to find a \mathbf{T} where $d'_k \ll d_k$ that minimizes the approximation error. A natural framework for finding such a transformation \mathbf{T} is Principal Component Analysis (PCA). By computing the empirical covariance matrix $\hat{\Sigma} = \frac{1}{N} \sum_t \mathbf{k}_t \mathbf{k}_t^\top$ over a calibration set, we can derive a projection matrix \mathbf{T} from the top- d'_k eigenvectors. This transformation rotates the state-space to maximize the preserved key variance. While theoretically optimal for reconstruction by the Eckart-Young-Mirsky Theorem (Eckart & Young, 1936; Mirsky, 1960), this approach produces a dense transformation matrix. In addition, as we will outline in the subsequent paragraph, it is not compatible out of the box with current linear attention architectures.

The Convolution Constraint. To achieve actual wall-clock speedup, \mathbf{T} must be absorbed into the weight matrices \mathbf{W}_K and \mathbf{W}_Q . However, linear attention models typically employ depthwise separable convolutions (So et al., 2021; Fu et al., 2022; Yang et al., 2023; Gu & Dao, 2024; Dao & Gu, 2024; Yang et al., 2024b) immediately after the input projections (see Algorithm 2 in the Appendix for a prototypical DeltaNet layer). While the sequence mixer is compatible with orthogonal transformations (Proposition 3.1), depthwise convolutions are not. A general dense semi-orthogonal matrix \mathbf{T} (such as one derived from PCA) would mix channels and thus misalign them with their corresponding convolution filters. Preserving the dynamics under such rotations would require converting the efficient diagonal convolution filters into expensive dense matrices. Therefore, we constrain our search to *axis-aligned* transformations. The case of general orthogonal matrices is discussed in Appendix B.4.

3.3. Axis-Aligned Methods

To circumvent intricacies related to convolutions, we restrict our focus to transformations that preserve the channel-wise

¹A semi-orthogonal matrix $\mathbf{T} \in \mathbb{R}^{d'_k, d_k}$ with $d'_k \leq d_k$ satisfies $\mathbf{T}\mathbf{T}^\top = \mathbf{I}_{d'_k}$.

convolutions. Formally, this restricts transformations to *axis-aligned* semi-orthogonal matrices:

Definition 3.2 (Axis-Aligned Transformations). Let $\mathcal{I} = \{i_1, \dots, i_{d'_k}\} \subseteq \{1, \dots, d_k\}$ be a set of distinct indices with cardinality $d'_k < d_k$. We define the axis-aligned projection matrix $\mathbf{P}_{\mathcal{I}} \in \mathbb{R}^{d'_k, d_k}$ as the matrix whose rows are the standard basis vectors corresponding to \mathcal{I} :

$$\mathbf{P}_{\mathcal{I}} = \begin{bmatrix} \mathbf{e}_{i_1}^\top \\ \vdots \\ \mathbf{e}_{i_{d'_k}}^\top \end{bmatrix}.$$

This matrix is semi-orthogonal. Applying it corresponds to a structural pruning operation that selects the subset of channels \mathcal{I} and discards the rest. Crucially, this operation preserves the independence of the remaining channels:

Proposition 3.3 (Compatibility with Depthwise Convolutions). *Let $\text{Conv1D}(\mathbf{X}, \mathbf{W})$ denote a depthwise convolution on input $\mathbf{X} \in \mathbb{R}^{T, d_k}$ with per-channel filters $\mathbf{W} \in \mathbb{R}^{d_k, l}$ of size l . Let $\mathbf{P}_{\mathcal{I}}$ be an axis-aligned semi-orthogonal transformation. Then:*

$$\text{Conv1D}(\mathbf{X}, \mathbf{W})\mathbf{P}_{\mathcal{I}}^\top = \text{Conv1D}(\mathbf{X}\mathbf{P}_{\mathcal{I}}^\top, \mathbf{P}_{\mathcal{I}}\mathbf{W}).$$

This result implies that key dimensions can be pruned by simply slicing the corresponding columns from the projection matrices \mathbf{W}_K and \mathbf{W}_Q , along with the corresponding entries of the convolution weights \mathbf{W} . In the following paragraphs, we present a plethora of different strategies to select the optimal index set \mathcal{I} for each head, ranging from simple magnitude-based heuristics to a novel rank-revealing approach. Recall that, by Proposition 3.1, every transformation must be applied to the queries and keys *simultaneously*. To satisfy this requirement and to capture interactions between memory and queries, the proposed column selection mechanisms incorporate both queries and keys.

Weight-Magnitude-based (L^1). As a baseline, we implement a weight-magnitude based pruner, defining the importance of the j -th channel as the sum of the l^1 norms of the corresponding columns in the query and key projection matrices: $s_j = \|\mathbf{W}_{Q,:j}\|_1 + \|\mathbf{W}_{K,:j}\|_1$. We rank these scores locally within each head and select the top- d'_k indices to form the retained set \mathcal{I} .

S-Wanda. We adapt Wanda (Sun et al., 2023a) to our structured setting (coining the method *S-Wanda*), defining the saliency of the j -th channel by aggregating the element-wise Wanda scores across the input channel dimension. Specifically, we sum the product of weight magnitudes and input feature norms over a calibration set:

$$s_j = \sum_{i=1}^h (|\mathbf{W}_{Q,ij}| + |\mathbf{W}_{K,ij}|) \|\mathbf{X}_{:i}\|_2,$$

where $\|\mathbf{X}_{:,i}\|_2$ is the l^2 norm of the i -th input feature computed over a small calibration set. Unlike L^1 , this metric accounts for the distribution of the input.

Sensitivity-based. We employ a gradient-based saliency criterion (LeCun et al., 1989; Wang et al., 2019; Ma et al., 2023) to identify dimensions that maximally influence the training objective. It is the only method we consider that takes into account information beyond the current layer and is task-aware. We quantify the importance of the j -th key dimension using the first-order Taylor expansion of the loss on a calibration set:

$$s_j = \sum_i (|\mathbf{W}_{\mathbf{Q},ij} \nabla_{\mathbf{w}_{\mathbf{Q},ij}} \mathcal{L}| + |\mathbf{W}_{\mathbf{K},ij} \nabla_{\mathbf{w}_{\mathbf{K},ij}} \mathcal{L}|).$$

Rank-based (DRRQR). In light of our theoretical insights into the role of rank in linear attention models (Section 2.2.2), we propose an algorithm that explicitly improves the conditioning of the queries and keys. By Proposition 2.2, this increases the effective rank of the associative memory. *Deep Rank Revealing QR (DRRQR)* applies a *Strong Rank Revealing QR* factorization (Gu & Eisenstat, 1996) to the activation statistics $\mathbf{M} = [\mathbf{K}, \mathbf{Q}] \in \mathbb{R}^{2N, d_k}$ to select a subset of d'_k columns that form a well-conditioned set of channels. The algorithm (see Algorithm 1) starts from a QR decomposition with column pivoting and then iteratively permutes columns between a current chosen basis and a set of candidates to satisfy numerical stability bounds; we detail the specific swap-gain metric and update rules in Appendix B.2. This procedure guarantees that the leading triangular factor $\mathbf{A}_{d'_k}$ is well-conditioned. By explicitly lower-bounding $\sigma_{\min}(\mathbf{A}_{d'_k})$, *DRRQR* minimizes $\kappa(\mathbf{A}_{d'_k})$ and thus implicitly maximized rank utilization (see Proposition D.5 in the Appendix). Unlike heuristic approaches, *DRRQR* relies on deterministic bounds for rank revelation, rendering the method tractable and interpretable.

4. Related Work

Rank Considerations. Rank collapse is a well-known phenomenon in transformers. Dong et al. (2021) show that skip connections help alleviate it, while Noci et al. (2022) show that collapsed queries and keys hinder gradient flow at initialization. In this work, we tie the rank of the queries and keys to that of the hidden state in linear attention, showing how a skewed spectrum of the associative memory can amplify query noise during readout.

Recent empirical results furthermore imply that linear attention models do not manage their associative memory well (Siems et al., 2025; Parnichkun et al., 2025), indicating that the memory of linear attention models often exhibits a low-rank structure. Our work builds on these observations, forcing the model to operate in a lower-dimensional space at

Algorithm 1 Compact version of Deep Rank Revealing QR (DRRQR). The full algorithm may be found Algorithm 3.

```

1: Input: Matrix  $\mathbf{M} \in \mathbb{R}^{2N, d_k}$ , Rank  $d'_k$ , Tolerance  $f \geq 1$ 
2: Output: Selected Indices  $\mathcal{I}$ 
3:
4:  $[\mathbf{Q}, \mathbf{R}, \mathbf{\Pi}] \leftarrow \text{QRCP}(\mathbf{M})$ 
5: Partition  $\mathbf{R} = \begin{pmatrix} \mathbf{A}_{d'_k} & \mathbf{B}_{d'_k} \\ \mathbf{0} & \mathbf{C}_{d'_k} \end{pmatrix}$ , where  $\mathbf{A}_{d'_k} \in \mathbb{R}^{d'_k, d'_k}$ 
6: Init  $\omega_i(\mathbf{A}_{d'_k}) = \|(\mathbf{A}_{d'_k}^{-1})_{i,:}\|_2^{-1}$ ,  $\gamma_j(\mathbf{C}_{d'_k}) = \|(\mathbf{C}_{d'_k})_{:,j}\|_2$ 
7:
8: while True do
9:   Compute  $\mathbf{U} = \mathbf{A}_{d'_k}^{-1} \mathbf{B}_{d'_k}$ 
10:
11:  if  $\rho_{\arg\max_{i,j} \sqrt{|U_{ij}|^2 + (\gamma_j(\mathbf{C}_{d'_k})/\omega_i(\mathbf{A}_{d'_k}))^2}} \leq f$  then
12:    break
13:  end if
14:
15:  Swap col  $i^*$  of  $\begin{pmatrix} \mathbf{A}_{d'_k} \\ \mathbf{0} \end{pmatrix}$  with col  $j^*$  of  $\begin{pmatrix} \mathbf{B}_{d'_k} \\ \mathbf{C}_{d'_k} \end{pmatrix}$ 
16:  Update  $\mathbf{R}$ ,  $\omega(\mathbf{A}_{d'_k})$ , and  $\gamma(\mathbf{C}_{d'_k})$ 
17: end while
18:
19: Return:  $\mathbf{\Pi}[1 : d'_k]$ 

```

increased *rank utilization* and minimal decrease in *effective rank* (Ipsen & Saibaba, 2025).

Pruning Methods. Most pruning methods are unstructured or semi-structured (LeCun et al., 1989; Frantar & Alistarh, 2023; Sun et al., 2023a) and thus require specialized kernels to realize sparsity-induced speedups. SparseGPT (Frantar & Alistarh, 2023) frames pruning as a local reconstruction problem. Wanda (Sun et al., 2023a) proposes a simpler, gradient-free metric based on the product of weight magnitudes and input activation norms. Several works have sought to enhance this metric by re-incorporating second-order information or gradients. GBLM (Das et al., 2023) and Pruner-Zero (Dong et al., 2024) utilize gradients derived from full-model backpropagation to refine pruning scores. Wanda++ (Yang et al., 2025) introduces regional gradients computed at the decoder-block level to decrease the computational cost.

A fundamental challenge in structured pruning is the handling of coupled structures, where removing a neuron or head in one layer breaks dimensional consistency in subsequent layers. Ma et al. (2023) (LLM-Pruner) address this by constructing dependency graphs to identify groups of parameters that must be excised simultaneously. Similarly, our work addresses the structural coupling of linear attention models, specifically the dependency between the projection matrices of queries and keys and the depthwise convolutions.

SliceGPT (Ashkboos et al., 2024a) applies structured pruning to the residual stream by pruning, for example, the rows of query and key weight matrices. In particular, the attention mechanism still lives in the same space pre- and post-slicing. Our work can thus be considered complementary to this approach. By pruning columns, we explicitly reduce the dimension of the attention mechanism.

Quantization Methods. Recent quantization approaches like QuaRot (Ashkboos et al., 2024b) and SpinQuant (Liu et al., 2024) apply an orthogonal matrix to the residual stream to disperse large outliers, creating more quantization-friendly distributions. Crucially, this rotation is structurally absorbed into the model weights: the rotation applied to the activations is counteracted by applying the inverse rotation to the subsequent weight matrices. As a result, the projections produce the same queries, keys, and values as the unquantized model (up to quantization errors), rendering the sequence mixer unaware of the rotation applied to the residual stream.

5. Experiments

We use the *flame* (Zhang & Yang, 2025) library for recovery fine-tuning (RFT, Ashkboos et al. (2024a)) and pre-training the 370M parameter models. RFT uses LoRA (Hu et al., 2022) on a single H100 GPU. The details on our experimental setup may be found in Appendix A. Besides the state reduction methods introduced in Section 3, we also report a *Rand* baseline which randomly selects an index set to use for dropping query and key columns.

Table 2. Pre-RFT Performance of Gated DeltaNet models at 50% compression, evaluated using Wikitext and Lambada perplexities.

METHOD	370M		1.3B	
	WIKI	LMB	WIKI	LMB
L1	41.8	156.6	26.5	34.0
RAND	35.5	50.7	18.8	14.4
S-WANDA	40.0	141.5	21.9	24.1
GRAD	<u>33.3</u>	39.2	<u>17.4</u>	10.1
DRRQR	31.6	<u>39.4</u>	17.3	<u>14.2</u>
Base	28.8	35.9	16.8	9.7

5.1. Results

We evaluate the introduced structured pruning methods on DeltaNet (Yang et al., 2024b) and Gated DeltaNet (Yang et al., 2024a) at 370M and 1.3B parameter scales. Specifically, we compare the optimization-based approaches, *DRRQR* (rank-optimal) and *Grad* (gradient-based), with the magnitude-based pruning methods.

Figure 2 shows the typical rank utilization during a forward

pass through DeltaNet 370M at a compression ratio of 75%. We can see that the two most powerful compression methods, *Grad* and *DRRQR*, have the largest rank utilization.

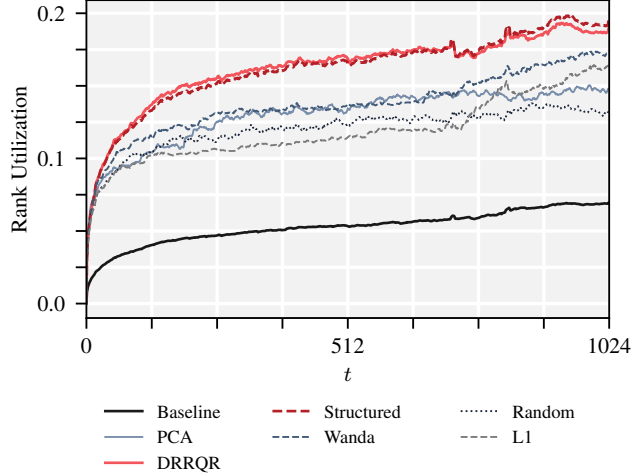


Figure 2. Rank utilization of DeltaNet 370M as a function of the token index for a random sample of Fineweb-Edu of length 1024, averaged over layers and heads, at a compression ratio of 75% pre-RFT. Note how the strongest models exhibit the largest rank utilization. All models except for the baseline have the same maximum capacity and are thus directly comparable.

Language Modeling. We observe that pruning 50% of the key dimension entails minimal degradation in Wikitext2 and Lambada perplexity, especially when using the *Grad* and *DRRQR* pruners, even before RFT (see Table 2). For example, Gated DeltaNet 1.3B sees Wikitext perplexity go from 16.8 to 17.4 at 50% compression ratio. Even at 75%, the perplexity only goes up by about two points. This finding suggests that pre-trained linear attention models seem to effectively use at most half of their available capacity for next token prediction.

We generally find the rank-based method *DRRQR* to perform competitively with the gradient-saliency based *Grad*, even though it is local and task-agnostic. *Grad*, on the other hand, is non-local and removes weight in a way that entails a minimal increase in perplexity. This highlights the influence of our rank considerations on model performance.

Table 1 contains extended post-RFT results for the specific case of Gated DeltaNet 1.3B. More comprehensive breakdowns are provided in Tables 8-16 in the Appendix.

The zero-shot common sense reasoning scores remain robust under compression. For instance, Gated DeltaNet 1.3B maintains an average of 58.3 at 50% compression when compressed via *Grad*, around a one-point drop from the 59.4 baseline. The retrieval tasks show higher sensitivity to state reduction, especially *FDA* and *SWDE*. However, for more conservative pruning ratios around 30%, the retrieval capabilities stay competitive.

Table 1. Comprehensive post-RFT evaluation of Gated DeltaNet 1.3B. We report Wikitext and Lambada perplexities, the average zero-shot generation accuracy (ZS, Gao et al. (2024)) as well as average retrieval accuracy (Ret, Arora et al. (2024)) across varying compression ratios (best results in **bold**, second best underlined).

METHOD	75% COMPRESSION				50% COMPRESSION				40% COMPRESSION				30% COMPRESSION							
	WIKI		LMB	ZS	RED	WIKI		LMB	ZS	RED	WIKI		LMB	ZS	RED	WIKI		LMB	ZS	RED
	↓	↓	↑	↑	↓	↓	↓	↓	↑	↑	↓	↓	↑	↑	↑	↓	↓	↑	↑	↑
RAND	19.3	18.1	54.6	23.9	16.9	<u>11.5</u>	57.8	32.1	16.5	<u>10.7</u>	58.3	34.6	<u>16.1</u>	<u>10.2</u>	58.7	<u>37.3</u>				
L1	18.6	16.8	55.3	25.7	16.8	13.0	57.2	32.9	16.5	11.9	57.8	34.6	16.3	11.3	58.3	35.4				
S-WANDA	18.2	15.1	55.4	26.2	16.6	11.7	57.8	<u>33.2</u>	16.4	11.5	58.1	34.4	16.1	11.0	58.6	37.2				
GRAD	17.8	12.5	56.8	26.9	<u>16.4</u>	10.5	58.3	34.3	16.1	10.1	<u>58.6</u>	35.8	15.9	9.9	59.0	38.0				
DRRQR	<u>17.9</u>	<u>14.7</u>	<u>56.2</u>	<u>26.1</u>	16.3	12.0	<u>58.0</u>	33.0	16.1	11.0	58.7	35.0	15.9	10.7	<u>58.8</u>	36.5				
BASELINE	16.8	9.7	59.4	40.3																

A Note on PCA. Our theoretical analysis in Section 3 suggests a problem with PCA due to misaligned causal convolutions. Our experiments empirically validate those claims, finding that PCA-based pruning generally underperforms axis-aligned methods. We provide a detailed discussion and experiments in Appendix C.2.

Ablation on the Coupled Selection. We investigate the impact of selecting pruning targets based on just keys, just queries, or both. Our ablation study (detailed in Appendix C.3) reveals that magnitude-based heuristics (*L1*, *S-Wanda*) are unstable when targeting keys, performing best when restricted to queries. In contrast, the two best methods, *Grad* and *DRRQR*, consistently achieve the lowest perplexity using joint selection. Note that for fair comparability, all extensive results in this paper (Section 5.1) use joint selection for all methods. However, even if we compare the optimal configuration for heuristics (queries-only) against our proposed methods (joint), *Grad* and *DRRQR* still demonstrate superior performance, confirming that optimization-based approaches successfully capture the coupled read/write interaction that heuristics miss.

Table 3. Training throughput (TPS, tokens per second) of sequence mixers on an NVIDIA H100 (batch size 32, sequence length 2048, number of heads 16, hidden dimension 2048). We fix the value expansion factor at 1.0 and vary the per-head key dimension d_k .

Model	d_k	TPS	Speedup	Memory	Ratio
DeltaNet	128	8.1M	1.00×	6.33GiB	1.00
	64	10.8M	1.34×	4.57GiB	0.72
	32	12.9M	1.60×	3.70GiB	0.58
Gated DeltaNet	128	7.9M	1.00×	6.35GiB	1.00
	64	10.4M	1.32×	4.59GiB	0.72
	32	12.2M	1.55×	3.71GiB	0.58

Speedup. Our structured pruning methods apply a joint semi-orthogonal projection to the keys and queries, effectively reducing the per-head key dimension from d_k to a rank $d'_k < d_k$. Mathematically, this transforms the original

dynamical system into another dynamical system with a reduced state $\mathbf{S}' \in \mathbb{R}^{d_v, d'_k}$. We benchmark the sequence mixer throughput and peak VRAM usage on an NVIDIA H100 GPU (see Table 3). Comparing the baseline ($d_k = 128$) against compressed variants ($d_k \in \{64, 32\}$): For DeltaNet, a 50% reduction yields approximately a 1.33× speedup in terms of throughput. A 75% reduction yields a speedup of ≈ 1.58×. Peak VRAM usage decreases by 28% and 42%, respectively.

6. Discussion

Motivated by the low-rank structure of the associative memory in trained linear attention models, we propose a state-size reduction framework that selects a subset of informative key and query columns while discarding the remainder. In addition to adapting several heuristic pruning strategies to this framework, we introduce a principled structured pruning method explicitly designed to improve effective rank and rank utilization. We further provide a rigorous analysis of the role of rank in linear attention, showing that low-rank structure can amplify query noise and govern retrieval error. Finally, we present extensive empirical evaluations demonstrating the practical efficiency and effectiveness of our structured pruning framework.

Our empirical results show that the sequence mixer can be compressed by up to 50% while incurring only a minor increase in perplexity. However, our findings also highlight a limitation of the proposed framework: reducing the state size can lead to performance drops on recall-intensive tasks. This observation is well known for linear attention models (Arora et al., 2024) and is a primary motivation for hybrid architectures that combine linear and softmax attention. Accordingly, a promising direction for future work would be to apply our structured pruning approach to hybrid models, where the additional softmax attention layers may help mitigate performance losses on recall-intensive tasks.

Impact Statement

This paper presents work whose goal is to advance the field of Machine Learning. There are many potential societal consequences of our work, none of which we feel must be specifically highlighted here.

Acknowledgements

PN is supported by the Max Planck ETH Center for Learning Systems. This work was supported in part by the Hector Foundation.

The authors would like to thank Shlomo Libo Feigin, Neehal Tumma, Sajad Movahedi, Timur Carstensen, Patrik Wolf, Heinrich Campe, and Benedict Armstrong for the interesting discussions and valuable feedback on this work.

References

Arora, S., Timalsina, A., Singhal, A., Eyuboglu, S., Zhao, X., Rao, A., Rudra, A., and Ré, C. Just Read Twice: Closing the Recall Gap for Recurrent Language Models. *arXiv preprint arXiv:2407.05483*, 2024.

Ashkboos, S., Croci, M. L., Nascimento, M. G. d., Hoefler, T., and Hensman, J. SliceGPT: Compress Large Language Models by Deleting Rows and Columns. *arXiv preprint arXiv:2401.15024*, 2024a.

Ashkboos, S., Mohtashami, A., Croci, M. L., Li, B., Cameron, P., Jaggi, M., Alistarh, D., Hoefler, T., and Hensman, J. Quarot: Outlier-Free 4-bit Inference in Rotated LLMs. *Advances in Neural Information Processing Systems*, 37:100213–100240, 2024b.

Blakeman, A., Basant, A., Khattar, A., Renduchintala, A., Bercovich, A., Ficek, A., BJORLIN, A., Taghibakhshi, A., Deshmukh, A. S., Mahabaleshwaran, A. S., et al. Nemotron-H: A Family of Accurate and Efficient Hybrid Mamba-Transformer Models. *arXiv preprint arXiv:2504.03624*, 2025.

Chen, C.-T. *Linear System Theory and Design*. Saunders college publishing, 1984.

Dao, T. and Gu, A. Transformers are SSMs: Generalized Models and Efficient Algorithms through Structured State Space Duality. *arXiv preprint arXiv:2405.21060*, 2024.

Das, R. J., Sun, M., Ma, L., and Shen, Z. Beyond Size: How Gradients Shape Pruning Decisions in Large Language Models. *arXiv preprint arXiv:2311.04902*, 2023.

Dong, P., Li, L., Tang, Z., Liu, X., Pan, X., Wang, Q., and Chu, X. Pruner-Zero: Evolving Symbolic Pruning Metric from Scratch for Large Language Models. *arXiv preprint arXiv:2406.02924*, 2024.

Dong, Y., Cordonnier, J.-B., and Loukas, A. Attention is not All You Need: Pure Attention Loses Rank Doubly Exponentially with Depth. In *International conference on machine learning*, pp. 2793–2803. PMLR, 2021.

Eckart, C. and Young, G. The Approximation of One Matrix by Another of Lower Rank. *Psychometrika*, 1(3):211–218, 1936.

Frantar, E. and Alistarh, D. SparseGPT: Massive Language Models Can Be Accurately Pruned in One-Shot. In *International conference on machine learning*, pp. 10323–10337. PMLR, 2023.

Fu, D. Y., Dao, T., Saab, K. K., Thomas, A. W., Rudra, A., and Ré, C. Hungry Hungry Hippos: Towards Language Modeling with State Space Models. *arXiv preprint arXiv:2212.14052*, 2022.

Gao, L., Tow, J., Abbasi, B., Biderman, S., Black, S., DiPofi, A., Foster, C., Golding, L., Hsu, J., Le Noac'h, A., Li, H., McDonell, K., Muennighoff, N., Ociepa, C., Phang, J., Reynolds, L., Schoelkopf, H., Skowron, A., Sutawika, L., Tang, E., Thite, A., Wang, B., Wang, K., and Zou, A. The Language Model Evaluation Harness, 07 2024. URL <https://zenodo.org/records/12608602>.

Gu, A. and Dao, T. Mamba: Linear-Time Sequence Modeling with Selective State Spaces. In *First conference on language modeling*, 2024.

Gu, M. and Eisenstat, S. C. Efficient Algorithms for Computing a Strong Rank-Revealing QR Factorization. *SIAM Journal on Scientific Computing*, 17(4):848–869, 1996.

Hu, E. J., Shen, Y., Wallis, P., Allen-Zhu, Z., Li, Y., Wang, S., Wang, L., Chen, W., et al. LoRA: Low-Rank Adaptation of Large Language Models. In *International Conference on Learning Representations*, 2022.

Hua, W., Dai, Z., Liu, H., and Le, Q. Transformer Quality in Linear Time. In *International conference on machine learning*, pp. 9099–9117. PMLR, 2022.

Ipsen, I. C. and Saibaba, A. K. Stable Rank and Intrinsic Dimension of Real and Complex Matrices. *SIAM Journal on Matrix Analysis and Applications*, 46(3):1988–2007, 2025.

Katharopoulos, A., Vyas, A., Pappas, N., and Fleuret, F. Transformers are RNNs: Fast Autoregressive Transformers with Linear Attention. In *International conference on machine learning*, pp. 5156–5165. PMLR, 2020.

LeCun, Y., Denker, J., and Solla, S. Optimal Brain Damage. *Advances in neural information processing systems*, 2, 1989.

Li, A., Gong, B., Yang, B., Shan, B., Liu, C., Zhu, C., Zhang, C., Guo, C., Chen, D., Li, D., et al. Minimax-01: Scaling Foundation Models with Lightning Attention. *arXiv preprint arXiv:2501.08313*, 2025.

Lieber, O., Lenz, B., Bata, H., Cohen, G., Osin, J., Dalmedigos, I., Safahi, E., Meirom, S., Belinkov, Y., Shalev-Shwartz, S., et al. Jamba: A Hybrid Transformer-Mamba Language Model. *arXiv preprint arXiv:2403.19887*, 2024.

Lingle, L. D. Transformer-VQ: Linear-Time Transformers via Vector Quantization. *arXiv preprint arXiv:2309.16354*, 2023.

Liu, Z., Zhao, C., Fedorov, I., Soran, B., Choudhary, D., Krishnamoorthi, R., Chandra, V., Tian, Y., and Blankevoort, T. SpinQuant: LLM Quantization with Learned Rotations. *arXiv preprint arXiv:2405.16406*, 2024.

Ma, X., Fang, G., and Wang, X. LLM-Pruner: On the Structural Pruning of Large Language Models. *Advances in neural information processing systems*, 36:21702–21720, 2023.

Mirsky, L. Symmetric Gauge Functions and Unitarily Invariant Norms. *The quarterly journal of mathematics*, 11 (1):50–59, 1960.

Noci, L., Anagnostidis, S., Biggio, L., Orvieto, A., Singh, S. P., and Lucchi, A. Signal Propagation in Transformers: Theoretical Perspectives and the Role of Rank Collapse. *Advances in Neural Information Processing Systems*, 35: 27198–27211, 2022.

Parnichkun, R. N., Tumma, N., Thomas, A. W., Moro, A., An, Q., Suzuki, T., Yamashita, A., Poli, M., and Masaroli, S. Quantifying Memory Utilization with Effective State-Size. *arXiv preprint arXiv:2504.19561*, 2025.

Peng, B., Alcaide, E., Anthony, Q., Albalak, A., Arcadinho, S., Biderman, S., Cao, H., Cheng, X., Chung, M., Grella, M., et al. RWKV: Reinventing RNNs for the Transformer Era. *arXiv preprint arXiv:2305.13048*, 2023.

Pope, R., Douglas, S., Chowdhery, A., Devlin, J., Bradbury, J., Heek, J., Xiao, K., Agrawal, S., and Dean, J. Efficiently scaling transformer inference. *Proceedings of machine learning and systems*, 5:606–624, 2023.

Rudelson, M. and Vershynin, R. Sampling from Large Matrices: An Approach through Geometric Functional Analysis. *Journal of the ACM (JACM)*, 54(4):21–es, 2007.

Schlag, I., Irie, K., and Schmidhuber, J. Linear Transformers Are Secretly Fast Weight Programmers. In *International conference on machine learning*, pp. 9355–9366. PMLR, 2021.

Siems, J., Carstensen, T., Zela, A., Hutter, F., Pontil, M., and Grazzi, R. DeltaProduct: Improving State-Tracking in Linear RNNs via Householder Products. *arXiv preprint arXiv:2502.10297*, 2025.

So, D., Mańke, W., Liu, H., Dai, Z., Shazeer, N., and Le, Q. V. Searching for Efficient Transformers for Language Modeling. *Advances in neural information processing systems*, 34:6010–6022, 2021.

Sun, M., Liu, Z., Bair, A., and Kolter, J. Z. A Simple and Effective Pruning Approach for Large Language Models. *arXiv preprint arXiv:2306.11695*, 2023a.

Sun, Y., Dong, L., Huang, S., Ma, S., Xia, Y., Xue, J., Wang, J., and Wei, F. Retentive Network: A Successor to Transformer for Large Language Models. *arXiv preprint arXiv:2307.08621*, 2023b.

Team, K., Zhang, Y., Lin, Z., Yao, X., Hu, J., Meng, F., Liu, C., Men, X., Yang, S., Li, Z., et al. Kimi Linear: An Expressive, Efficient Attention Architecture. *arXiv preprint arXiv:2510.26692*, 2025.

Team, Q. Qwen3-Next: Towards Ultimate Training & Inference Efficiency, 2025.

Trefethen, L. N. and Bau, D. *Numerical Linear Algebra*. SIAM, 2022.

Tropp, J. A. et al. An Introduction to Matrix Concentration Inequalities. *Foundations and Trends® in Machine Learning*, 8(1-2):1–230, 2015.

Vaswani, A., Shazeer, N., Parmar, N., Uszkoreit, J., Jones, L., Gomez, A. N., Kaiser, Ł., and Polosukhin, I. Attention Is All You Need. *Advances in neural information processing systems*, 30, 2017.

Vershynin, R. *High-Dimensional Probability: An Introduction with Applications in Data Science*, volume 47 of *Cambridge Series in Statistical and Probabilistic Mathematics*. Cambridge University Press, 2018.

Wang, C., Grosse, R., Fidler, S., and Zhang, G. Eigendamage: Structured Pruning in the Kronecker-Factored Eigenbasis. In *International conference on machine learning*, pp. 6566–6575. PMLR, 2019.

Yang, S., Wang, B., Shen, Y., Panda, R., and Kim, Y. Gated Linear Attention Transformers with Hardware-Efficient Training. *arXiv preprint arXiv:2312.06635*, 2023.

Yang, S., Kautz, J., and Hatamizadeh, A. Gated Delta Networks: Improving Mamba2 with Delta Rule. *arXiv preprint arXiv:2412.06464*, 2024a.

Yang, S., Wang, B., Zhang, Y., Shen, Y., and Kim, Y. Parallelizing Linear Transformers with the Delta Rule over Sequence Length. *Advances in neural information processing systems*, 37:115491–115522, 2024b.

Yang, Y., Zhen, K., Ganesh, B., Galstyan, A., Huybrechts, G., Müller, M., Kübler, J. M., Swaminathan, R. V., Mouchtaris, A., Bodapati, S. B., et al. Wanda++: Pruning Large Language Models via Regional Gradients. *arXiv preprint arXiv:2503.04992*, 2025.

Zhang, Y. and Yang, S. Flame: Flash Language Modeling Made Easy, January 2025. URL <https://github.com/fla-org/flame>.

A. Training Details

We use the *flame* (Zhang & Yang, 2025) library for recovery fine-tuning (RFT, Ashkboos et al. (2024a)) and pre-training the 370M parameter models. The latter uses 10 billion tokens of Fineweb-Edu. The larger DeltaNet and Gated DeltaNet models are taken from fla-hub ² and m-a-p ³, respectively.

We perform RFT on a single H100 GPU using LoRA (Hu et al., 2022) with rank $r = 16$ $\alpha = 32$, using $32k$ samples of Fineweb-Edu. During training, we use: a batch size of 16, training on sequences of length 2048. After warming up for 5% of the total steps, we decay the learning rate from 10^{-4} down to 10^{-5} . We furthermore unfreeze the causal convolutions, which make up just a fraction of the total parameters. As suggested by Ma et al. (2023), we furthermore apply knowledge-distillation during RFT using the original model.

For the compression methods requiring a calibration set, we use 128 samples of Fineweb-Edu. *DRRQR* uses a random subsample of $5k$ keys and queries each.

B. Additional Material

Algorithm 2 describes a typical DeltaNet (Yang et al., 2024b) layer.

Algorithm 2 A Typical DeltaNet Layer

```

1: Input: Hidden states  $\mathbf{X} \in \mathbb{R}^{T,d}$ , Previous state  $\mathbf{S}_0$ 
2: Parameters:  $\mathbf{W}_q, \mathbf{W}_k \in \mathbb{R}^{d_k, h}, \mathbf{W}_v \in \mathbb{R}^{d_v, h}, \mathbf{W}_o \in \mathbb{R}^{h, d_v}, \mathbf{W}_\beta \in \mathbb{R}^{1, h}$ .
3:
4: // 1. Projections and Local Mixing (Short Convolutions)
5:  $\mathbf{q} \leftarrow \text{SiLU}(\text{Conv1D}(\mathbf{X}\mathbf{W}_q))$ 
6:  $\mathbf{k} \leftarrow \text{SiLU}(\text{Conv1D}(\mathbf{X}\mathbf{W}_k))$ 
7:  $\mathbf{v} \leftarrow \text{SiLU}(\text{Conv1D}(\mathbf{X}\mathbf{W}_v))$ 
8:  $\beta \leftarrow \sigma(\mathbf{X}\mathbf{W}_\beta)$ 
9:
10: // 2. Normalization
11:  $\mathbf{q} \leftarrow \mathbf{q}/\|\mathbf{q}\|_2$ 
12:  $\mathbf{k} \leftarrow \mathbf{k}/\|\mathbf{k}\|_2$ 
13:
14: // 3. Delta Rule
15: for  $t = 1$  to  $T$  do
16:    $\mathbf{S}_t \leftarrow \mathbf{S}_{t-1}(\mathbf{I} - \beta_t \mathbf{k}_t \mathbf{k}_t^\top) + \beta_t \mathbf{v}_t \mathbf{k}_t^\top$ 
17:    $\mathbf{o}_t \leftarrow \mathbf{S}_t \mathbf{q}_t$ 
18: end for
19: Concatenate heads to form  $\mathbf{O} \in \mathbb{R}^{T,d}$ 
20:
21: // 4. Output Projection
22:  $\mathbf{O} \leftarrow \text{RMSNorm}(\mathbf{O})$ 
23:  $\mathbf{Y} \leftarrow \mathbf{O}\mathbf{W}_o$ 
24:
25: Return:  $\mathbf{Y}$ 

```

B.1. Structured Pruning from the Test-Time Regression Perspective

Linear attention, and specifically DeltaNet, are usually interpreted as performing gradient descent on a linear regression objective (Schlag et al., 2021; Yang et al., 2024b), where the hidden state \mathbf{S}_t acts as the fast weight matrix trained to map keys \mathbf{k}_t (inputs) to values \mathbf{v}_t (targets). In this framework, our proposed structured pruning strategy admits another interpretation, functioning as a *feature selection* step applied to the input of the online learner. By restricting the input features to the subspace spanned by the transformation matrix \mathbf{T} , we effectively constrain the hypothesis class of the regression. This forces the fast weights to ignore the null space of \mathbf{T} , acting as a form of regularization.

²<https://huggingface.co/collections/fla-hub/deltanet>

³<https://huggingface.co/m-a-p/1.3B-100B-GatedDeltaNet-pure>

Algorithm 3 Deep Rank Revealing QR (*DRRQR*). Adapted from Algorithm 4 of Gu & Eisenstat (1996).

```

1: Input: Activation Matrix  $\mathbf{A} \in \mathbb{R}^{2N, d_k}$ , Target Rank  $d'_k$ , Tolerance  $f \geq 1$ 
2: Output: Selected Indices  $\mathcal{I}$ 
3:
4: // 1. Initialization: QR with Column Pivoting
5:  $[\mathbf{Q}, \mathbf{R}, \boldsymbol{\Pi}] \leftarrow \text{QRCP}(\mathbf{A})$ 
6: Partition  $\mathbf{R} = \begin{pmatrix} \mathbf{A}_{d'_k} & \mathbf{B}_{d'_k} \\ \mathbf{0} & \mathbf{C}_{d'_k} \end{pmatrix}$ , where  $\mathbf{A}_{d'_k} \in \mathbb{R}^{d'_k, d'_k}$ 
7: Initialize  $\omega_i(\mathbf{A}_{d'_k}) = 1/\|(\mathbf{A}_{d'_k}^{-1})_{i,:}\|_2$  and  $\gamma_j(\mathbf{C}_{d'_k}) = \|(\mathbf{C}_{d'_k})_{:,j}\|_2$ 
8:
9: // 2. Iterative Swapping for Stability
10: while True do
11:   Compute  $\mathbf{U} = \mathbf{A}_{d'_k}^{-1} \mathbf{B}_{d'_k}$ 
12:
13:   // Calculate swap gain metric  $\rho_{ij}$  for all pairs
14:   // Checks if  $U_{ij}$  is large or if residual  $\gamma_j$  is large relative to basis  $\omega_i$ 
15:    $\rho_{ij} \leftarrow \sqrt{|U_{ij}|^2 + (\gamma_j(\mathbf{C}_{d'_k})/\omega_i(\mathbf{A}_{d'_k}))^2}$ 
16:
17:   Let  $(i^*, j^*) = \text{argmax}_{i,j} \rho_{ij}$ 
18:   if  $\rho_{i^*j^*} \leq f$  then
19:     break // Strong RRQR condition met
20:   end if
21:
22:   Swap column  $i^*$  of  $\mathbf{A}_{d'_k}$  with column  $j^*$  of  $\mathbf{C}_{d'_k}$ 
23:   Update  $\mathbf{R}$ ,  $\omega(\mathbf{A}_{d'_k})$ , and  $\gamma(\mathbf{C}_{d'_k})$ 
24: end while
25:
26:  $\mathcal{I} \leftarrow \boldsymbol{\Pi}[1 : d'_k]$ 
27: Return:  $\mathcal{I}$ 

```

B.2. Details on Rank Revealing QR (RRQR)

In this section, we detail the *Strong Rank-Revealing QR* (RRQR) algorithm (see Algorithm 3) proposed by Gu & Eisenstat (1996), which forms the basis of our *DRRQR* pruning method.

Mathematical Formulation. Let $\mathbf{M} \in \mathbb{R}^{m,n}$ be the input matrix of concatenated keys and queries (in the main text, $m = 2N$ and $n = d_k$). We seek a permutation $\boldsymbol{\Pi}$ and a target rank k (in our main text denoted as d'_k) such that the QR factorization

$$\mathbf{M}\boldsymbol{\Pi} = \mathbf{Q} \begin{pmatrix} \mathbf{A}_k & \mathbf{B}_k \\ \mathbf{0} & \mathbf{C}_k \end{pmatrix} \quad (7)$$

satisfies specific bounds on the singular values of the leading principal submatrix $\mathbf{A}_k \in \mathbb{R}^{k,k}$ and the trailing submatrix $\mathbf{C}_k \in \mathbb{R}^{(m-k), (n-k)}$. Specifically, a Strong RRQR factorization guarantees that $\sigma_{\min}(\mathbf{A}_k)$ is bounded away from zero and $\|\mathbf{C}_k\|_2 = \sigma_{\max}(\mathbf{C}_k)$ is small. This implies that \mathbf{A}_k is well-conditioned.

Geometric Intuition. The algorithm aims to select k columns that maximize the volume of the parallelotope formed by the selected column vectors. Since $|\det(\mathbf{A}_k)| = \prod_{i=1}^k \sigma_i(\mathbf{A}_k)$, maximizing the determinant pushes the smallest singular values upward, thereby minimizing the condition number $\kappa(\mathbf{A}_k)$.

The Swap Criterion. Let $\boldsymbol{\Pi}$ be the current permutation column permutation matrix. To determine if swapping the i -th column of the basis (where $1 \leq i \leq k$) with the j -th column of the residual (where $1 \leq j \leq n - k$) improves the factorization, we analyze the ratio of the new determinant to the current determinant.

Gu & Eisenstat (1996) derive an efficiently computable metric for this ratio. Let $\mathbf{U} = \mathbf{A}_k^{-1} \mathbf{B}_k$. We define:

- $\gamma_j(\mathbf{C}_k) = \|(\mathbf{C}_k)_{:,j}\|_2$: The ℓ_2 -norm of the j -th column of the residual block.
- $\omega_i(\mathbf{A}_k) = 1/\|(\mathbf{A}_k^{-1})_{i,:}\|_2$: The reciprocal of the ℓ_2 -norm of the i -th row of the inverse basis.

By Lemma 3.1 of Gu & Eisenstat (1996), the potential gain ρ_{ij} from swapping basis column i with candidate column j is given by:

$$\rho_{ij} = \sqrt{|U_{ij}|^2 + \left(\frac{\gamma_j(\mathbf{C}_k)}{\omega_i(\mathbf{A}_k)}\right)^2}. \quad (8)$$

If $\rho_{ij} > f$ for a chosen tolerance factor $f \geq 1$, swapping these columns guarantees an increase in $|\det(\mathbf{A}_k)|$ by a factor of at least ρ_{ij} . The first term, $|U_{ij}|^2$, captures the linear dependence of the candidate vector on the current basis vector, while the second term captures the magnitude of the candidate relative to the stability of the basis vector.

Algorithm and Update Rules. The *DRRQR* procedure (Algorithm 3) proceeds as follows:

1. **Initialization:** Compute an initial factorization using standard QRCP. This provides a baseline $\mathbf{\Pi}$, \mathbf{A}_k , \mathbf{B}_k , and \mathbf{C}_k .
2. **Identification:** Search for a pair of indices (i, j) such that $\rho_{ij} > f$. Efficient search strategies maximize over j for fixed i , or simply identify the first valid pair.
3. **Update:** If a valid pair is found:
 - (a) Permute columns to swap indices i and $j + k$.
 - (b) Retriangularize the matrix \mathbf{R} using Givens rotations to restore the upper-triangular structure of \mathbf{A}_k . This costs $O(k(n - k))$ operations rather than the $O(n^3)$ of a full factorization.
 - (c) Update the auxiliary vectors $\omega(\mathbf{A}_k)$ and $\gamma(\mathbf{C}_k)$ using the formulas provided in Section 4 of Gu & Eisenstat (1996).
4. **Termination:** The process repeats until no pair (i, j) satisfies $\rho_{ij} > f$, ensuring the matrix satisfies the strong rank-revealing condition.

B.3. Derivation of Tighter Error Bounds

In this section, we derive tighter bounds for the retrieval error ratio. The proof of Theorem 2.5 relies on the loose upper bound $\|\mathbf{S}\mathbf{n}\|_2 \leq \|\mathbf{S}\|_F \|\mathbf{n}\|_2$.

However, if we allow using the condition number $\kappa(\mathbf{S}) = \sigma_1/\sigma_d$ as a measure for the anisotropy of the associative memory, it follows readily from standard perturbation theory that

$$\frac{1}{\kappa(\mathbf{S})} \leq \frac{\|\mathbf{o} - \mathbf{o}^*\|_2 / \|\mathbf{o}^*\|_2}{\|\mathbf{n}\|_2 / \|\mathbf{q}^*\|_2} \leq \kappa(\mathbf{S}). \quad (9)$$

Indeed, it holds that (Trefethen & Bau, 2022, Lecture 12) $\sigma_d \|\mathbf{x}\|_2 \leq \|\mathbf{S}\mathbf{x}\|_2 \leq \sigma_1 \|\mathbf{x}\|_2$ for any vector \mathbf{x} . Applying these inequalities to $\mathbf{S}\mathbf{n}$ and $\mathbf{S}\mathbf{q}^*$ yields Equation (9). Similar to Corollary 2.6, this allows deriving bounds on the expected error under isotropic Gaussian noise (assuming again $\|\mathbf{q}^*\|_2 = 1$ for simplicity):

$$\frac{1}{\kappa(\mathbf{S})} \mu \leq \|\mathbf{o} - \mathbf{o}^*\|_2 / \|\mathbf{o}^*\|_2 \leq \kappa(\mathbf{S}) \mu.$$

B.4. Adapting Convolutions to General Rotations

Handling the more general case of (semi-) orthogonal, non-axis-aligned transformations is more intricate than the axis-aligned one (see Section 3.3). In particular, Proposition 3.3 does not hold anymore. If one wishes to employ general orthogonal transformations $\mathbf{T} \in O(d_k)$ (such as those derived from PCA) to prune the sequence mixer, the convolution layers must be adapted.

Depthwise convolutions operate independently on each channel. When the input space is rotated via \mathbf{T} , the original basis-aligned filters become misaligned with the new principal components. Towards maintaining learned structures after pruning, one must find new convolution kernels that best approximate the original dynamics.

B.5. Optimal Diagonal Adaptation

We formalize this adaptation as an optimization problem: finding the optimal diagonal (channel-wise) filters in the new basis that minimize the reconstruction error of the original convolution output.

Proposition B.1 (Optimal Diagonal Adaptation). *Let \mathbf{x}_t be the input signal and let $\mathbf{T} \in O(d)$ be an orthogonal matrix, yielding features $\tilde{\mathbf{x}}_t = \mathbf{T}\mathbf{x}_t$. Let $\mathbf{W} \in \mathbb{R}^{d,l}$ be the original learnable filters for d channels and kernel size l .*

The optimal diagonal per-channel weights $\mathbf{W}' \in \mathbb{R}^{d,l}$ that minimize the expected squared reconstruction error:

$$\min_{\mathbf{W}'} \mathbb{E}_{\mathbf{x}} \left[\|\mathbf{W}' * \tilde{\mathbf{x}} - \mathbf{T}(\mathbf{W} * \mathbf{x})\|_F^2 \right]$$

are given by the energy-weighted projection:

$$\mathbf{W}' = (\mathbf{T} \odot \mathbf{T})\mathbf{W},$$

where $$ denotes the depthwise convolution and \odot is the Hadamard (element-wise) product.*

Proof. We seek to find new depthwise separable convolutions with filter weights \mathbf{W}' that minimize the error between the rotated input convolved with the new weights and the rotated original output.

Recall that a depthwise convolution with filter matrix \mathbf{W}' acting on input $\tilde{\mathbf{x}}$ can be written as:

$$\mathbf{W}' * \tilde{\mathbf{x}} = \sum_{j=0}^{l-1} \mathbf{W}'^{(j)} \tilde{\mathbf{x}}_{t-j},$$

where $\mathbf{W}'^{(j)} = \text{diag}(\mathbf{w}'^{(j)})$ is the diagonal filter matrix at time lag j . Similarly, the rotated original output is:

$$\mathbf{T}(\mathbf{W} * \mathbf{x}) = \mathbf{T} \sum_{j=0}^{l-1} \mathbf{W}^{(j)} \mathbf{x}_{t-j} = \sum_{j=0}^{l-1} \mathbf{T}\mathbf{W}^{(j)}\mathbf{T}^\top \tilde{\mathbf{x}}_{t-j},$$

where we used $\mathbf{x} = \mathbf{T}^\top \tilde{\mathbf{x}}$.

The error term is then $\sum_{j=0}^{l-1} (\mathbf{W}'^{(j)} - \mathbf{T}\mathbf{W}^{(j)}\mathbf{T}^\top) \tilde{\mathbf{x}}_{t-j}$. Thus, the ideal filter in the new basis is the dense matrix $\mathbf{M}^{(j)} := \mathbf{T}\mathbf{W}^{(j)}\mathbf{T}^\top$. However, to maintain the efficiency of depthwise convolutions, we are constrained to approximate this dense matrix with a diagonal matrix $\mathbf{W}'^{(j)}$.

Let us focus on the error for a specific lag j (omitting j for brevity) and channel k . The error vector is $\mathbf{e} = (\mathbf{W}' - \mathbf{M})\tilde{\mathbf{x}}$. The k -th component is:

$$e_k = (W'_{kk} - M_{kk})\tilde{x}_k - \sum_{n \neq k} M_{kn}\tilde{x}_n.$$

Squaring and taking the expectation, assuming the features in the rotated basis $\tilde{\mathbf{x}}$ are decorrelated (which is true if \mathbf{T} is the PCA transformation matrix) such that $\mathbb{E}[\tilde{x}_k \tilde{x}_n] = 0$ for $n \neq k$:

$$\mathbb{E}[e_k^2] = (W'_{kk} - M_{kk})^2 \mathbb{E}[\tilde{x}_k^2] + \sum_{n \neq k} M_{kn}^2 \mathbb{E}[\tilde{x}_n^2].$$

To minimize this error with respect to the diagonal weight W'_{kk} , we must set the first term to zero:

$$W'_{kk} = M_{kk} = (\mathbf{T} \text{ diag}(\mathbf{w}) \mathbf{T}^\top)_{kk}.$$

Expanding this matrix multiplication:

$$W'_{kk} = \sum_{m=1}^d T_{km} w_m T_{km} = \sum_{m=1}^d (T_{km})^2 w_m = ((\mathbf{T} \odot \mathbf{T})\mathbf{w})_k.$$

Extending this to all channels and lags, we obtain the matrix form $\mathbf{W}' = (\mathbf{T} \odot \mathbf{T})\mathbf{W}$. \square

Intuitively, the new kernel for a principal component is a weighted average of the original kernels, weighted by the energy (squared contribution) each original dimension contributes to that component.

B.6. Shared Convolutions

An alternative approach to facilitate general rotations is to constrain the model architecture itself. If we enforce that the convolution filters are shared across all channels within a head, the convolution operation becomes a scalar multiplication at each lag, which commutes with any linear transformation.

Lemma B.2 (Commutativity of Shared Convolutions). *Let $\mathbf{w} \in \mathbb{R}^l$ be a filter shared across all d channels, such that the convolution kernel matrix $\mathbf{W} \in \mathbb{R}^{d,l}$ has identical rows $\mathbf{W}_{k,:} = \mathbf{w}$ for all k . For any linear transformation matrix $\mathbf{T} \in \mathbb{R}^{d,d}$ (including orthogonal rotations), the convolution commutes with the transformation:*

$$\mathbf{W} * (\mathbf{T}\mathbf{x}) = \mathbf{T}(\mathbf{W} * \mathbf{x}).$$

Proof. For a shared filter, the convolution operation on the vector \mathbf{x}_t can be written as a scalar convolution applied element-wise: $(\mathbf{W} * \mathbf{x})_t = \sum_{j=0}^{l-1} w_j \mathbf{x}_{t-j}$. Applying the transformation \mathbf{T} first:

$$\mathbf{W} * (\mathbf{T}\mathbf{x})_t = \sum_{j=0}^{l-1} w_j (\mathbf{T}\mathbf{x}_{t-j}) = \mathbf{T} \left(\sum_{j=0}^{l-1} w_j \mathbf{x}_{t-j} \right) = \mathbf{T}(\mathbf{W} * \mathbf{x})_t.$$

□

This lemma implies that for models trained with shared convolutions, the optimal filter in the rotated basis \mathbf{W}' is identical to the original filter \mathbf{W} . This architectural choice would render the model naturally robust to basis changes, enabling rotation-based pruning methods like PCA-based truncation without the need for filter adaptation or approximation errors.

C. Additional Experimental Results

C.1. Singular Value Spectrum

Figure 3 depicts the singular value spectrum of a randomly selected head. We compare the uncompressed baseline against the DRRQR and Grad methods at a 75% compression ratio prior to recovery fine-tuning (pre-RFT). Notably, the uncompressed model exhibits a long tail of vanishingly small singular values, whereas the compressed models display a more truncated spectrum.

Figure 4 illustrates the impact of recovery fine-tuning on the spectrum. We observe that the fine-tuning process diffuses the singular value distribution, effectively softening the sharp spectral cutoff by re-introducing smaller singular values.

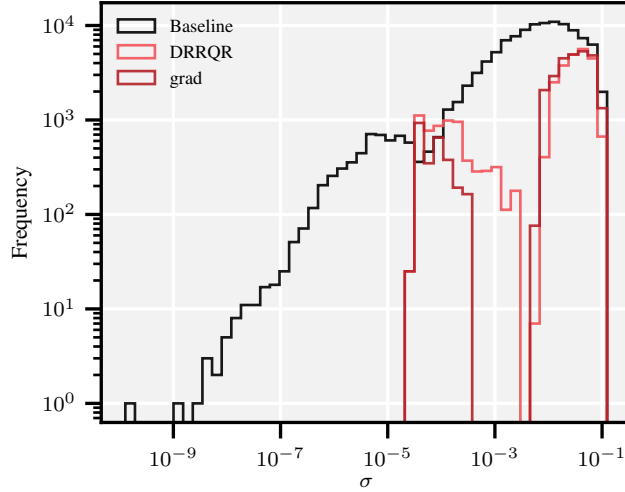


Figure 3. Singular value distribution of a DeltaNet 370M layer computed on a random Fineweb-Edu sample ($T = 1024$). We compare the uncompressed *Baseline* against *DRRQR* and *Grad* at 75% compression (pre-RFT).

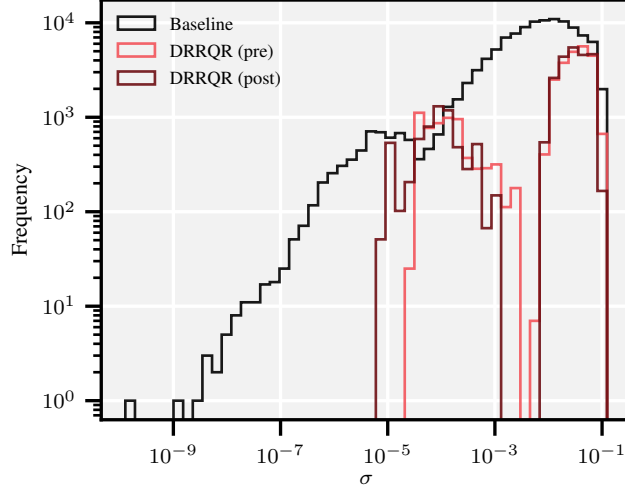


Figure 4. Impact of Recovery Fine-Tuning (RFT) on the singular value spectrum. We compare the uncompressed *Baseline* against *DRRQR* at 75% compression, both before (*pre*) and after (*post*) RFT.

C.2. On PCA and Convolutions

In this section, we provide extended experimental results on the PCA-based pruning strategy. We furthermore analyze the impact of depthwise convolutions on the applicability and performance of semi-orthogonal structured pruning.

As mentioned in Section 3, depthwise convolutions are generally not invariant under orthogonal transformations. When pruning via PCA, the features are rotated, causing a misalignment with the per-channel convolution filters. In Appendix B.4, we lay out a framework to fix this misalignment, either by introducing *shared convolutions* or by *mixing filters* (see Proposition B.1).

C.2.1. SHARED CONVOLUTIONS

To understand the impact of those two approaches, we train DeltaNet 370M variants using *Shared Convolutions*, where the convolution filter is tied across all channels within a head. As shown in Lemma B.2, this architecture is equivariant under rotations.

Table 4. DeltaNet 370M models trained on 10B tokens evaluated on common sense zero-shot reasoning tasks. “Shared Conv” indicates whether convolution filters are shared across heads and/or channels (for example, $\times\checkmark$ means that filters are shared across channels inside a head but not across heads).

Shared Conv	Wiki. ppl \downarrow	LMB. ppl \downarrow	ARC-e acc. n \uparrow	ARC-c acc. n \uparrow	Hella. acc. n \uparrow	Wino. acc \uparrow	PIQA acc. n \uparrow	LMB. acc \uparrow	Avg \uparrow
$\times\times$	29.8	37.0	51.1	27.6	38.1	52.2	65.0	31.3	44.2
$\times\checkmark$	29.5	40.4	49.7	27.1	38.3	52.4	64.7	30.4	43.8
$\checkmark\checkmark$	29.3	40.4	49.9	26.4	37.8	49.9	65.2	29.9	43.2

Filter Similarity. Figure 5 visualizes the learned filters of a standard DeltaNet (non-shared). We observe high similarity between filters within specific heads, suggesting that the model naturally learns to share dynamics across channels. This could serve as a justification for sharing filters among channels inside each head.

Performance of Shared Convolutions. We include results on pre-trained DeltaNet models with and without shared convolutions in Table 4. It shows that, while models with shared convolutions are competitive (especially when just shared inside of a head and not across heads), there is a slight drop-off.

Table 5. Comparison of post-compression (pre-RFT) perplexity on Wikitext-2 for DeltaNet 370M. We compare standard (Non-Shared) vs. Shared Convolutions under different pruning strategies. "PCA (adv.)" removes the highest variance components (keeping noise), while "PCA (prop.)" removes the lowest variance components (keeping signal).

Comp.	Method	Non Shared	Shared
75%	PCA (adv.)	$3.1 \cdot 10^5$	$2.1 \cdot 10^5$
	PCA (prop.)	$3.3 \cdot 10^5$	184.48
	Grad	46.7	69.78
50%	PCA (adv.)	$2.4 \cdot 10^5$	$6.1 \cdot 10^4$
	PCA (prop.)	$3.2 \cdot 10^5$	155.76
	Grad	31.75	33.73
0%	–	29.83	29.55

Table 6. Consolidated ablation study on DeltaNet and Gated DeltaNet models (370M and 1.3B) measuring Wikitext-2 perplexity. We compare the impact of picking just keys (**K**), just queries (**Q**), or both (**K, Q**) for feature selection at a 50% compression ratio.

Method	DeltaNet						Gated DeltaNet					
	370M			1.3B			370M			1.3B		
	K, Q	K	Q	K, Q	K	Q	K, Q	K	Q	K, Q	K	Q
L1	3843.5	425218.3	33.0	66.1	1596.3	34.9	41.8	61.0	49.9	26.5	29.75	24.5
DRRQR	31.4	286035.7	32.1	20.5	566.9	22.9	31.6	56.9	43.5	17.3	21.9	22.0
Grad	31.7	17709.6	31.9	18.3	20.3	19.5	33.3	36.2	34.6	17.4	18.3	17.7
S-Wanda	915.9	376074.0	33.0	60.0	1604.4	29.1	40.0	61.3	43.5	21.9	22.5	21.5
Baseline	29.8			16.7			28.8			16.8		

C.2.2. IMPACT OF CONVOLUTIONS ON PCA-BASED PRUNING

Towards quantifying the two approaches of handling the per-channel convolutions, we compare a "Proper PCA" method, where we retain the principal components with the highest variance, against an "Adversarial PCA" baseline, where we deliberately retain the dimensions with the lowest variance. In a system robust to rotation, proper PCA should outperform the adversarial baseline.

Table 5 presents the perplexity on Wikitext-2 for DeltaNet 370M (pre-RFT). For the shared convolutions, proper PCA generally yields way better perplexity than the adversarial baseline. However, in the standard, non-shared case, the filter averaging does not suffice to make up for the misalignment post-transformation. Furthermore, the *Grad* pruning methods still outperforms PCA even when using shared convolutions.

C.3. On Coupled Selection

We compare selecting indices based on (i) the sum of scores derived from both projections (**K, Q**), (ii) keys only (**K**), and (iii) queries only (**Q**). Results are reported in Table 6.

We observe that selecting columns based on query projections (**Q**) consistently outperforms selection based solely on keys (**K**) for magnitude-based methods. Since queries govern retrieval, pruning based on **Q** ensures we discard dimensions with minimal contribution to the output. In contrast, pruning based on **K** risks removing information that the model attempts to access with a strong query, leading to significant readout errors.

Curiously, magnitude-based methods seem to perform better when selecting just based on queries (**Q**) than when selecting based on both keys and queries (**K, Q**). Since they add the scores of keys and queries ($s_j = \|\mathbf{W}_{k,:j}\| + \|\mathbf{W}_{q,:j}\|$), this suggests the model contains large key weights whose corresponding query weights have lower magnitude.

DRRQR avoids this by targeting the effective rank of the joint subspace.

The results in Table 6 reveal a clear difference between the studied pruning methods. Magnitude-based methods (*L1*, *Wanda*) are unstable when targeting keys, performing best when restricted to queries. In contrast, optimization-based methods (*Grad*, *DRRQR*) consistently achieve the lowest perplexity using joint selection (**K, Q**). This indicates that the associative memory's effective rank requires accounting for the coupled interaction between keys and queries, rather than treating them

in isolation.

D. The Effective Rank

In this section we present some properties of the effective rank. For more details, please refer to (Ipsen & Saibaba, 2025).

Definition D.1 (effective rank). For a non-zero matrix $\mathbf{A} \in \mathbb{R}^{m,n}$, the effective rank is defined as:

$$\text{sr}(\mathbf{A}) := \frac{\|\mathbf{A}\|_F^2}{\|\mathbf{A}\|_2^2} = \frac{\sum_i \sigma_i^2(\mathbf{A})}{\sigma_{\max}^2(\mathbf{A})}.$$

Unlike the algebraic rank, which is discontinuous, the effective rank is a continuous function of the matrix entries. This implies that small perturbations to the memory state \mathbf{S}_t (e.g., from gradient noise or quantization) result in bounded changes to $\text{sr}(\mathbf{S}_t)$.

Proposition D.2 (Invariance under Transposition). *The effective rank is invariant under transposition. For any matrix \mathbf{A} :*

$$\text{sr}(\mathbf{A}) = \text{sr}(\mathbf{A}^\top).$$

Proposition D.3 (Invariance under Unitary Transformations and Scaling). *The effective rank is invariant under unitary transformations and scalar multiplication. For any unitary matrices \mathbf{U}, \mathbf{V} and non-zero scalar $c \in \mathbb{R}$:*

$$\text{sr}(c\mathbf{U}\mathbf{A}\mathbf{V}^\top) = \text{sr}(\mathbf{A}).$$

Proposition D.4 (Bounds and Relation to Algebraic Rank). *The effective rank is bounded by the algebraic rank:*

$$1 \leq \text{sr}(\mathbf{A}) \leq \text{rank}(\mathbf{A}) \leq \min(m, n).$$

The lower bound is achieved if and only if \mathbf{A} has rank 1. The upper bound is achieved if and only if all non-zero singular values are equal.

Proposition D.5 (Relation to Condition Number). *Let \mathbf{A} be a (non-zero) matrix. Then*

$$\kappa^2(\mathbf{A}) \geq \frac{\text{rank}(\mathbf{A})}{\text{sr}(\mathbf{A})}.$$

In the specific case where \mathbf{A} has full rank, this implies

$$\kappa^2(\mathbf{A}) \geq \frac{1}{u(\mathbf{A})},$$

where u is the rank utilization (see Definition 2.3).

Edge Case (Isotropy): In the specific case where the matrix is perfectly conditioned on its support (i.e., $\kappa(\mathbf{A}) = 1$), the inequality becomes an equality:

$$1 \geq \frac{r}{\text{sr}(\mathbf{A})} \implies \text{sr}(\mathbf{A}) \geq r.$$

Since we known $\text{sr}(\mathbf{A}) \leq r$, this forces $\text{sr}(\mathbf{A}) = \text{rank}(\mathbf{A})$. This confirms that for isotropic matrices (where all non-zero singular values are equal), the effective rank and algebraic rank coincide. Conversely, a large gap between r and $\text{sr}(\mathbf{A})$ is a sufficient condition for ill-conditioning.

E. Dynamical Systems Perspective

In this section, we derive the DeltaNet recurrence rule from a continuous-time dynamical systems perspective. We show that the sequence mixer can be interpreted as a discretization of a continuous gradient flow minimizing a linear regression objective.

Continuous-Time Dynamics. Consider a time-continuous associative memory $\mathbf{S}(t) \in \mathbb{R}^{d_v, d_k}$ receiving a stream of keys $\mathbf{k}(t) \in \mathbb{R}^{d_k}$ and values $\mathbf{v}(t) \in \mathbb{R}^{d_v}$. We define the instantaneous regression loss at time t as:

$$\mathcal{L}(\mathbf{S}(t)) = \frac{1}{2} \|\mathbf{v}(t) - \mathbf{S}(t)\mathbf{k}(t)\|_2^2.$$

The dynamics of the state $\mathbf{S}(t)$ are governed by the gradient flow minimizing this objective:

$$\dot{\mathbf{S}}(t) = -\nabla_{\mathbf{S}} \mathcal{L}(\mathbf{S}(t)) \quad (10)$$

$$= -(\mathbf{S}(t)\mathbf{k}(t) - \mathbf{v}(t))\mathbf{k}(t)^\top \quad (11)$$

$$= \mathbf{v}(t)\mathbf{k}(t)^\top - \mathbf{S}(t)\mathbf{k}(t)\mathbf{k}(t)^\top. \quad (12)$$

Equation (12) represents a linear time-varying (LTV) ordinary differential equation (ODE) of the form $\dot{\mathbf{S}}(t) = \mathbf{S}(t)\mathbf{A}(t) + \mathbf{B}(t)$, where $\mathbf{A}(t) = -\mathbf{k}(t)\mathbf{k}(t)^\top$ is the state-transition matrix acting on the right, and $\mathbf{B}(t) = \mathbf{v}(t)\mathbf{k}(t)^\top$ is the input forcing term.

Euler Discretization. To obtain the discrete-time update rule employed by DeltaNet, we apply the forward Euler method to Equation (12). Let Δt be the step size, which corresponds to the gating factor β_t in the DeltaNet formulation. The discretization yields:

$$\frac{\mathbf{S}_t - \mathbf{S}_{t-1}}{\beta_t} \approx \mathbf{v}_t \mathbf{k}_t^\top - \mathbf{S}_{t-1} \mathbf{k}_t \mathbf{k}_t^\top.$$

Rearranging the terms to solve for the next state \mathbf{S}_t :

$$\begin{aligned} \mathbf{S}_t &= \mathbf{S}_{t-1} + \beta_t (\mathbf{v}_t \mathbf{k}_t^\top - \mathbf{S}_{t-1} \mathbf{k}_t \mathbf{k}_t^\top) \\ &= \mathbf{S}_{t-1} (\mathbf{I} - \beta_t \mathbf{k}_t \mathbf{k}_t^\top) + \beta_t \mathbf{v}_t \mathbf{k}_t^\top. \end{aligned}$$

This exactly recovers the DeltaNet update rule (Equation (4)).

System Stability. The stability of this dynamical system is determined by the spectral properties of the transition matrix $(\mathbf{I} - \beta_t \mathbf{k}_t \mathbf{k}_t^\top)$. For the system to be stable (non-divergent), the eigenvalues of this operator must lie within the unit circle. This implies the condition $|1 - \beta_t \|\mathbf{k}_t\|_2^2| \leq 1$. In standard DeltaNet implementations, keys are normalized ($\|\mathbf{k}_t\|_2 = 1$), and β_t is the output of a sigmoid function ($\beta_t \in (0, 1)$), strictly satisfying the stability condition and ensuring the memory decays appropriately over time.

F. Proofs

In this section, we provide proofs of statements presented in the main paper.

F.1. Proof of Proposition 2.2

We consider the matrix form of the associative memory $\mathbf{S} = \mathbf{V}^\top \mathbf{K}$, where $\mathbf{V} \in \mathbb{R}^{T, d_v}$ and $\mathbf{K} \in \mathbb{R}^{T, d_k}$.

To handle potential misalignment between the subspaces of values and keys, we decompose the values \mathbf{V} into two orthogonal components relative to the column space of the keys \mathbf{K} :

$$\mathbf{V} = \mathbf{V}_{\parallel} + \mathbf{V}_{\perp},$$

where the columns of \mathbf{V}_{\parallel} lie in $\text{col}(\mathbf{K})$, and the columns of \mathbf{V}_{\perp} are orthogonal to it. Consequently, $\mathbf{V}_{\perp}^\top \mathbf{K} = \mathbf{0}$, and the memory state simplifies to:

$$\mathbf{S} = (\mathbf{V}_{\parallel} + \mathbf{V}_{\perp})^\top \mathbf{K} = \mathbf{V}_{\parallel}^\top \mathbf{K}.$$

We define the scalar quantity $\nu(\mathbf{V})$ appearing in the main text as the effective rank of the projected values:

$$\nu(\mathbf{V}) := \text{sr}(\mathbf{V}_{\parallel}) = \frac{\|\mathbf{V}_{\parallel}\|_F^2}{\|\mathbf{V}_{\parallel}\|_2^2}.$$

Since the columns of \mathbf{V}_{\parallel} lie entirely within the column space of \mathbf{K} , and assuming \mathbf{K} has full column rank, the matrix multiplication acts as a bijection on the row space of $\mathbf{V}_{\parallel}^{\top}$. We now derive the lower bound for the effective rank $\text{sr}(\mathbf{S}) = \|\mathbf{S}\|_F^2 / \|\mathbf{S}\|_2^2$.

First, we bound the numerator (Frobenius norm) from below. We use the property $\|\mathbf{AB}\|_F \geq \|\mathbf{A}\|_F \sigma_{\min}(\mathbf{B})$, which holds strictly here because the rows of $\mathbf{V}_{\parallel}^{\top}$ align with the range of \mathbf{K} :

$$\|\mathbf{S}\|_F^2 = \|\mathbf{V}_{\parallel}^{\top} \mathbf{K}\|_F^2 \geq \|\mathbf{V}_{\parallel}\|_F^2 \sigma_{\min}^2(\mathbf{K}).$$

Next, we bound the denominator (Spectral norm) from above using the standard sub-multiplicative property $\|\mathbf{AB}\|_2 \leq \|\mathbf{A}\|_2 \|\mathbf{B}\|_2$:

$$\|\mathbf{S}\|_2^2 = \|\mathbf{V}_{\parallel}^{\top} \mathbf{K}\|_2^2 \leq \|\mathbf{V}_{\parallel}\|_2^2 \|\mathbf{K}\|_2^2.$$

Combining these inequalities yields the lower bound:

$$\text{sr}(\mathbf{S}) = \frac{\|\mathbf{S}\|_F^2}{\|\mathbf{S}\|_2^2} \geq \frac{\|\mathbf{V}_{\parallel}\|_F^2 \sigma_{\min}^2(\mathbf{K})}{\|\mathbf{V}_{\parallel}\|_2^2 \|\mathbf{K}\|_2^2} = \text{sr}(\mathbf{V}_{\parallel}) \frac{1}{\kappa^2(\mathbf{K})} = \frac{\nu(\mathbf{V})}{\kappa^2(\mathbf{K})}.$$

□

F.2. Proof of Algebraic Rank

We first prove the following proposition:

Proposition F.1. *Let $\mathbf{S}_0 = 0$ and \mathbf{S}_t be a matrix satisfying the recursion*

$$\mathbf{S}_t = \mathbf{S}_{t-1}(\alpha_t \mathbf{I} - \beta_t \mathbf{k}_t \mathbf{k}_t^{\top}) + \gamma_t \mathbf{v}_t \mathbf{k}_t^{\top}$$

for some non-zero scalars $\alpha_t, \beta_t, \gamma_t$ and some vectors $\mathbf{v}_t, \mathbf{k}_t$. Then

$$\text{row } \mathbf{S}_t \subseteq \text{span}\langle \mathbf{k}_1, \dots, \mathbf{k}_t \rangle \quad \text{and} \quad \text{col } \mathbf{S}_t \subseteq \text{span}\langle \mathbf{v}_1, \dots, \mathbf{v}_t \rangle.$$

Consequently,

$$\text{rank } \mathbf{S}_t \leq \min(\text{rank } \mathbf{K}_t, \text{rank } \mathbf{V}_t)$$

where $\mathbf{K}_t = (\mathbf{k}_1, \dots, \mathbf{k}_t)$ and $\mathbf{V}_t = (\mathbf{v}_1, \dots, \mathbf{v}_t)$ are the matrices obtained by stacking the \mathbf{k} - and \mathbf{v} -vectors, respectively.

Proof. We start by showing the first claim by induction. For $t = 1$, we have $\mathbf{S}_1 = \gamma_1 \mathbf{v}_1 \mathbf{k}_1^{\top}$. Consider $t > 1$ and assume the claim is true for every $s < t$. Then

$$\begin{aligned} \mathbf{S}_t &= \mathbf{S}_{t-1}(\alpha_t \mathbf{I} - \beta_t \mathbf{k}_t \mathbf{k}_t^{\top}) + \gamma_t \mathbf{v}_t \mathbf{k}_t^{\top} \\ &= \alpha_t \mathbf{S}_{t-1} + (\gamma_t \mathbf{v}_t - \beta_t \mathbf{S}_{t-1} \mathbf{k}_t) \mathbf{k}_t^{\top} \\ &= \alpha_t \mathbf{S}_{t-1} + \mathbf{u}_t \mathbf{k}_t^{\top}, \end{aligned}$$

where we defined $\mathbf{u}_t := \gamma_t \mathbf{v}_t - \beta_t \mathbf{S}_{t-1} \mathbf{k}_t$. Next, we use that for two matrices \mathbf{A} and \mathbf{B} ,

$$\text{row}(\mathbf{A} + \mathbf{B}) \subseteq \text{span}(\text{row}(\mathbf{A}), \text{row}(\mathbf{B}))$$

and thus

$$\begin{aligned} \text{row}(\alpha_t \mathbf{S}_{t-1} + \mathbf{u}_t \mathbf{k}_t^{\top}) &\subseteq \text{span}(\text{row}(\alpha_t \mathbf{S}_{t-1}), \text{row}(\mathbf{u}_t \mathbf{k}_t^{\top})) \\ &= \text{span}(\text{row}(\mathbf{S}_{t-1}), \mathbf{k}_t) \\ &\subseteq \text{span}(\mathbf{k}_1, \dots, \mathbf{k}_t). \end{aligned}$$

This concludes the first claim.

For the second claim, we proceed analogously.

Indeed, we again show this claim by induction. The case $t = 1$ is clear. For any $t > 1$, we compute, using $\text{col}(\mathbf{AB}) \subseteq \text{col}(\mathbf{A})$,

$$\begin{aligned}\text{col}(\mathbf{S}_t) &= \text{col}(\mathbf{S}_{t-1}(\alpha_t \mathbf{I} - \beta_t \mathbf{k}_t \mathbf{k}_t^\top), \gamma_t \mathbf{v}_t \mathbf{k}_t^\top) \\ &\subseteq \text{col}(\mathbf{S}_{t-1}, \gamma_t \mathbf{v}_t \mathbf{k}_t^\top) \\ &\subseteq \text{col}(\mathbf{v}_1, \dots, \mathbf{v}_t).\end{aligned}$$

This concludes the proof. \square

Interestingly, PCA-based transformations are guaranteed to not decrease the rank of the keys:

Lemma F.2 (Monotonicity of Rank Utilization). *Pruning the low-variance directions via PCA strictly increases (or maintains) rank utilization. That is, for any $d'_k < d_k$:*

$$u(\mathbf{K}') \geq u(\mathbf{K}).$$

Proof. Assume towards a contradiction that the utilization decreases, i.e., $u(\mathbf{K}') < u(\mathbf{K})$. This means that

$$\frac{1}{d'_k} \sum_{i=1}^{d'_k} \sigma_i^2 < \frac{1}{d_k} \sum_{i=1}^{d_k} \sigma_i^2.$$

In words, the average energy of the top d'_k principal components is strictly less than the average energy of the full spectrum. This is a contradiction, as the singular values are non-increasing ($\sigma_1 \geq \dots \geq \sigma_{d_k}$). Thus, our assumption must have been wrong. \square

F.3. Proof of Theorem 2.5

We analyze the error amplification ratio R , defined as the relative output error divided by the input noise-to-signal ratio:

$$R = \frac{\|\mathbf{o} - \mathbf{o}^*\|_2 / \|\mathbf{o}^*\|_2}{\|\mathbf{n}\|_2 / \|\mathbf{q}^*\|_2} = \frac{\|\mathbf{Sn}\|_2}{\|\mathbf{n}\|_2} \cdot \frac{\|\mathbf{q}^*\|_2}{\|\mathbf{Sq}^*\|_2}.$$

This expression represents the Rayleigh quotient of the noise divided by the Rayleigh quotient of the signal.

We start by showing the lower bound. To find the minimum error, we start by projecting the response to the noise onto \mathbf{u}_1 :

$$\|\mathbf{Sn}\|_2 \geq |\mathbf{u}_1^\top \mathbf{Sn}| = \sigma_1 |\mathbf{w}_1^\top \mathbf{n}| = \sigma_1 \delta \|\mathbf{n}\|_2.$$

Next, we upper bound the response to the true signal, using Cauchy-Schwarz:

$$\|\mathbf{Sq}^*\|_2 \leq \|\mathbf{S}\|_F \|\mathbf{q}^*\|_2.$$

Substituting these into R :

$$R \geq \frac{\sigma_1 \delta \|\mathbf{n}\|_2}{\|\mathbf{n}\|_2} \cdot \frac{\|\mathbf{q}^*\|_2}{\|\mathbf{S}\|_F \|\mathbf{q}^*\|_2} = \delta \frac{\sigma_1}{\|\mathbf{S}\|_F} = \delta \frac{1}{\sqrt{\text{sr}(\mathbf{S})}}.$$

Using the definition $\text{sr}(\mathbf{S}) = d \cdot u(\mathbf{S})$, we obtain the lower bound:

$$R \geq \frac{\delta}{\sqrt{d \cdot u(\mathbf{S})}}.$$

Next, we show the upper bound. To find the maximum error, we first upper bound the response of the system to the noise:

$$\|\mathbf{Sn}\|_2 \leq \|\mathbf{S}\|_F \|\mathbf{n}\|_2.$$

Next, we lower bound the response to the true query by projecting onto \mathbf{u}_1 :

$$\|\mathbf{Sq}^*\|_2 \geq |\mathbf{u}_1^\top \mathbf{Sq}^*| = \sigma_1 |\mathbf{w}_1^\top \mathbf{q}^*| = \sigma_1 \gamma \|\mathbf{q}^*\|_2.$$

Table 7. Throughput measurements (thousands of tokens/second) and relative speedup factors for DeltaNet and Gated DeltaNet models on a single H100. Baselines (0%) are uncompressed models with head key dimension $d_k = 128$ for DeltaNet and $d_k = 256$ for Gated DeltaNet.

d_k	DeltaNet 370M		DeltaNet 1.3B		DeltaNet 2.7B		Gated DeltaNet 370M		Gated DeltaNet 1.3B	
	Throughput	Speedup	Throughput	Speedup	Throughput	Speedup	Throughput	Speedup	Throughput	Speedup
0%	416.2	1.00 \times	150.7	1.00 \times	81.5	1.00 \times	396.5	1.00 \times	138.4	1.00 \times
50%	474.8	1.14 \times	169.4	1.12 \times	91.7	1.12 \times	469.0	1.18 \times	157.8	1.14 \times
75%	505.9	1.22 \times	180.4	1.20 \times	98.6	1.21 \times	504.5	1.27 \times	170.1	1.22 \times
87.5%	521.6	1.25 \times	185.9	1.23 \times	99.3	1.22 \times	521.9	1.32 \times	176.3	1.26 \times

Again, substituting these into R :

$$R \leq \frac{\|\mathbf{S}\|_F \|\mathbf{n}\|_2}{\|\mathbf{n}\|_2} \cdot \frac{\|\mathbf{q}^*\|_2}{\sigma_1 \gamma \|\mathbf{q}^*\|_2} = \frac{1}{\gamma} \frac{\|\mathbf{S}\|_F}{\sigma_1} = \frac{\sqrt{\text{sr}(\mathbf{S})}}{\gamma}.$$

Using $\text{sr}(\mathbf{S}) = d \cdot u(\mathbf{S})$, we obtain the upper bound:

$$R \leq \frac{\sqrt{d \cdot u(\mathbf{S})}}{\gamma}.$$

□

F.4. Proof of Corollary 2.6

Follows by computing the bounds derived in Theorem 2.5. The noise follows $\mathbf{n} \sim \mathcal{N}(\mathbf{0}, \xi^2 \mathbf{I})$. Note that the expected norm of an isotropic Gaussian satisfies

$$\mu = \mathbb{E}[\|\mathbf{n}\|_2] = \xi \sqrt{2} \frac{\Gamma(\frac{d+1}{2})}{\Gamma(\frac{d}{2})}.$$

Furthermore, the expected alignment $z = \mathbf{w}_1^\top \mathbf{n}$ of an isotropic Gaussian \mathbf{n} with a vector \mathbf{w}_1 can be computed as

$$\mathbb{E}[\delta \|\mathbf{n}\|_2] = \mathbb{E}[|z|] = \xi \sqrt{\frac{2}{\pi}}.$$

□

G. Extended Results

G.1. Throughput Measurements

Table 7 shows the speedup achieved by compressing the state space. Compared to Table 3, it measures the throughput of the whole model during training, not just the sequence mixer layer.

G.2. Language Modeling

This subsection contains the extensive zero-shot (Gao et al., 2024) and real-world retrieval (Arora et al., 2024) task evaluations. Table 8 contains averaged results for all models at a fixed compression ratio of 50%. Tables 9-16.

Table 8. Comparison of compression methods at a 50% compression ratio pre-RFT across all model sizes, both pre- and post-RFT. We report Perplexity for WikiText2 (**Wiki**) and Lambada (**LMB**), as well as the average accuracy for Zero-Shot (**ZS**) and Retrieval (**Ret**) tasks (best results in **bold**, second best in underlined).

Model	Method	Pre-RFT			Post-RFT			
		Wiki ↓	LMB ↓	ZS Avg ↑	Wiki ↓	LMB ↓	ZS Avg ↑	Ret Avg ↑
DELTANET 370M	L1	3843.5	57304.8	33.0	32.5	56.8	43.0	15.8
	RAND	1032.6	2882.8	34.3	32.6	49.9	42.6	16.1
	DRRQR	31.4	<u>36.0</u>	<u>44.7</u>	29.4	<u>36.6</u>	44.5	17.8
	GRAD	<u>31.7</u>	33.3	44.9	29.4	36.3	<u>44.4</u>	<u>17.8</u>
	S-WANDA	915.9	6118.0	35.1	<u>32.1</u>	53.2	43.4	15.6
Baseline		29.8	37.0	44.2	29.8	37.0	44.2	20.8
DELTANET 1.3B	L1	66.1	298.7	41.6	19.0	16.1	48.2	29.1
	RAND	41.2	68.0	44.4	19.4	14.4	48.2	30.3
	DRRQR	<u>20.5</u>	47.2	<u>45.7</u>	<u>17.5</u>	<u>11.8</u>	<u>49.7</u>	<u>31.1</u>
	GRAD	18.3	15.4	48.8	17.2	11.3	50.3	33.3
	S-WANDA	60.0	361.3	40.8	18.5	15.9	48.3	28.9
Baseline		16.7	11.9	50.0	16.7	11.9	50.0	40.1
GATED DELTANET 370M	L1	41.8	156.6	40.4	29.2	44.6	43.5	18.1
	RAND	35.5	50.7	43.4	29.3	46.5	43.6	18.2
	DRRQR	31.6	<u>39.4</u>	44.0	28.7	<u>40.6</u>	43.8	<u>18.3</u>
	GRAD	<u>33.3</u>	39.2	<u>43.8</u>	28.7	39.4	<u>43.7</u>	19.0
	S-WANDA	40.0	141.5	40.9	<u>29.2</u>	44.6	<u>43.5</u>	18.2
Baseline		28.8	35.9	44.4	28.8	35.9	44.4	23.3
GATED DELTANET 1.3B	L1	26.5	34.0	53.3	16.8	13.0	57.2	32.9
	RAND	18.8	14.4	56.5	16.9	<u>11.5</u>	57.8	32.1
	DRRQR	17.3	<u>14.2</u>	<u>57.5</u>	16.3	12.0	<u>58.0</u>	33.0
	GRAD	<u>17.4</u>	10.1	58.6	<u>16.4</u>	10.5	58.3	34.3
	S-WANDA	21.9	24.1	55.1	16.6	11.7	57.8	<u>33.2</u>
Baseline		16.8	9.7	59.4	16.8	9.7	59.4	40.3

Table 9. Zero-shot performance of DeltaNet 370M models, evaluated using the *lm-eval-harness* (Gao et al., 2024), given different compression ratios. Pre- and post RFT.

RFT	Method	Compr.	Wiki. ppl ↓	LMB. ppl ↓	ARC-e acc_n ↑	ARC-c acc_n ↑	Hella. acc_n ↑	Wino. acc ↑	PIQA acc_n ↑	LMB. acc ↑	Avg ↑
✗	L1	75%	100083.0	9661610.6	27.2	28.0	27.7	52.2	50.9	0.0	31.0
✗	Rand	75%	136955.3	5879873.3	27.0	27.4	26.6	48.9	51.4	0.0	30.2
✗	DRRQR	75%	42.0	<u>74.1</u>	51.9	27.5	38.7	50.9	64.6	25.3	<u>43.1</u>
✗	Grad	75%	<u>46.7</u>	58.0	52.0	27.0	38.5	49.8	64.7	29.1	43.5
✗	S-Wanda	75%	33512.5	4955134.6	28.5	26.8	27.7	51.1	48.9	0.0	30
✓	L1	75%	36.3	146.7	46.0	26.2	36.1	51.0	63.0	17.1	39.9
✓	Rand	75%	40.3	129.9	46.8	26.1	35.8	51.9	62.8	17.7	40.2
✓	DRRQR	75%	31.4	<u>43.7</u>	52.0	27.5	38.1	52.4	64.6	29.7	<u>44.0</u>
✓	Grad	75%	<u>31.5</u>	42.5	52.1	28.0	38.0	51.6	64.8	30.2	44.1
✓	S-Wanda	75%	35.4	101.7	46.5	26.7	37.1	50.9	63.3	20.3	40.8
✗	L1	50%	3843.5	57304.8	35.8	23.6	31.2	50.8	55.0	1.6	33.0
✗	Rand	50%	1032.6	2882.8	37.8	23.7	30.3	50.5	56.6	6.9	34.3
✗	DRRQR	50%	31.4	<u>36.0</u>	52.1	27.6	38.7	52.0	65.1	32.7	<u>44.7</u>
✗	Grad	50%	<u>31.7</u>	33.3	51.8	27.9	38.7	52.2	65.5	33.4	44.9
✗	S-Wanda	50%	915.9	6118.0	39.9	24.3	33.5	50.1	57.4	5.4	35.1
✓	L1	50%	32.5	56.8	49.2	27.0	37.7	53.0	64.6	26.4	43.0
✓	Rand	50%	32.6	49.9	49.2	27.9	37.6	49.0	64.9	27.3	42.6
✓	DRRQR	50%	29.4	<u>36.6</u>	51.8	27.7	38.1	52.1	65.3	31.7	44.5
✓	Grad	50%	29.4	36.3	51.0	27.7	38.1	52.1	65.5	32.0	<u>44.4</u>
✓	S-Wanda	50%	32.1	53.2	51.1	26.1	37.9	52.6	65.0	27.7	43.4
✗	L1	40%	1232.0	5431.6	39.6	23.9	34.0	50.2	56.4	5.7	34.9
✗	Rand	40%	121.3	329.1	42.8	25.4	34.2	49.8	61.5	15.0	38.1
✗	DRRQR	40%	30.2	<u>33.4</u>	52.6	28.0	38.7	51.9	65.2	33.1	44.9
✗	Grad	40%	<u>30.4</u>	32.7	52.2	27.7	38.7	51.8	65.3	33.4	44.9
✗	S-Wanda	40%	276.8	603.4	45.3	25.4	35.8	50.3	60.3	13.4	38.4
✓	L1	40%	31.7	53.9	50.8	26.7	37.7	53.0	65.1	26.5	43.3
✓	Rand	40%	31.0	43.6	49.1	27.6	38.0	52.5	65.2	29.2	43.6
✓	DRRQR	40%	29.0	<u>36.3</u>	51.4	27.8	38.2	52.0	65.4	32.0	44.5
✓	Grad	40%	<u>29.1</u>	35.7	51.5	27.4	38.2	51.5	65.5	32.1	<u>44.4</u>
✓	S-Wanda	40%	31.2	48.3	50.7	26.9	38.0	52.4	64.8	28.8	43.6
✗	L1	30%	270.1	307.0	45.6	24.7	36.2	50.2	60.1	18.5	39.2
✗	Rand	30%	52.7	103.2	48.4	26.8	36.1	50.4	62.9	22.7	41.2
✗	DRRQR	30%	29.3	32.7	52.4	27.7	38.6	52.7	65.0	33.5	45.0
✗	Grad	30%	<u>29.4</u>	<u>33.0</u>	51.7	27.9	38.6	52.5	64.7	33.4	<u>44.8</u>
✗	S-Wanda	30%	138.9	133.9	46.3	26.0	37.1	50.0	62.0	22.7	40.7
✓	L1	30%	30.8	50.9	51.1	27.0	37.9	53.6	64.7	27.4	43.6
✓	Rand	30%	30.0	40.7	50.1	27.6	38.1	52.2	65.5	30.3	44.0
✓	DRRQR	30%	28.8	36.0	51.3	27.6	38.2	52.1	65.1	32.3	<u>44.4</u>
✓	Grad	30%	28.8	36.0	51.3	27.7	38.1	51.9	65.5	32.3	44.5
✓	S-Wanda	30%	30.7	45.4	51.2	27.2	38.0	52.6	64.9	29.6	43.9
Baseline	–	0%	29.8	37.0	51.1	27.6	38.1	52.2	65.0	31.3	44.2

Table 10. Zero-shot performance of DeltaNet 1.3B models, evaluated using the *lm-eval-harness* (Gao et al., 2024), given different compression ratios. Pre- and post RFT.

RFT	Method	Compr.	Wiki. ppl ↓	LMB. ppl ↓	ARC-e acc_n ↑	ARC-c acc_n ↑	Hella. acc_n ↑	Wino. acc ↑	PIQA acc_n ↑	LMB. acc ↑	Avg ↑
✗	L1	75%	2860.8	6728.9	36.0	26.4	41.5	51.9	62.4	2.6	36.8
✗	Rand	75%	53664.2	3585.3	37.4	26.9	36.5	50.2	60.3	3.6	35.8
✗	DRRQR	75%	43.9	375.5	43.6	27.7	49.1	51.3	69.5	9.9	41.8
✗	Grad	75%	27.0	61.5	49.7	27.0	49.3	52.3	69.8	22.4	45.1
✗	S-Wanda	75%	3160.0	6856.0	37.0	27.4	40.5	51.8	64.3	2.0	37.2
✓	L1	75%	20.2	26.6	48.1	25.8	47.3	51.1	68.7	33.1	45.7
✓	Rand	75%	22.9	22.9	47.8	27.1	46.5	51.5	69.7	35.3	46.3
✓	DRRQR	75%	19.2	17.5	50.5	27.3	48.7	53.5	69.6	40.5	48.4
✓	Grad	75%	19.0	14.7	50.7	26.8	49.1	52.4	69.9	43.6	48.8
✓	S-Wanda	75%	20.0	23.1	48.6	26.4	47.2	51.9	69.5	35.6	46.5
✗	L1	50%	66.1	298.7	42.4	27.2	47.9	54.4	67.1	10.6	41.6
✗	Rand	50%	41.2	68.0	46.9	27.8	47.9	53.7	69.5	20.4	44.4
✗	DRRQR	50%	20.5	47.2	46.5	27.8	51.3	53.0	69.9	25.5	45.7
✗	Grad	50%	18.3	15.4	48.8	27.5	50.9	53.4	70.2	42.2	48.8
✗	S-Wanda	50%	60.0	361.3	40.8	27.0	47.1	53.7	66.4	9.9	40.8
✓	L1	50%	19.0	16.1	48.9	27.1	48.6	53.7	69.7	41.1	48.2
✓	Rand	50%	19.4	14.4	48.5	26.2	48.6	52.5	69.9	43.4	48.2
✓	DRRQR	50%	17.5	11.8	51.0	26.6	49.7	53.3	69.7	48.2	49.7
✓	Grad	50%	17.2	11.3	51.2	26.5	49.9	54.5	70.7	48.7	50.3
✓	S-Wanda	50%	18.5	15.9	49.7	27.5	48.5	52.0	70.2	41.5	48.3
✗	L1	40%	45.2	194.4	44.1	27.3	48.2	53.8	68.5	13.6	42.6
✗	Rand	40%	23.9	30.0	49.3	27.6	49.1	52.3	69.3	30.6	46.4
✗	DRRQR	40%	19.3	37.8	47.8	28.3	52.0	54.4	69.5	28.4	46.7
✗	Grad	40%	17.9	13.0	48.8	26.9	51.0	53.5	70.3	45.6	49.4
✗	S-Wanda	40%	44.7	189.0	42.6	27.6	47.8	54.1	68.3	13.7	42.4
✓	L1	40%	18.5	13.7	49.8	27.1	48.8	52.2	69.8	44.6	48.7
✓	Rand	40%	18.6	13.0	49.6	26.4	48.9	52.8	70.2	44.8	48.8
✓	DRRQR	40%	17.1	11.1	51.5	27.0	49.9	53.9	69.7	49.2	50.2
✓	Grad	40%	17.1	10.4	50.8	26.8	50.1	54.5	70.7	50.8	50.6
✓	S-Wanda	40%	18.2	13.7	50.7	27.2	48.9	51.8	70.3	45.0	49.0
✗	L1	30%	37.6	128.6	44.5	27.1	48.7	53.4	68.6	16.6	43.2
✗	Rand	30%	19.8	22.9	48.9	27.3	49.3	53.7	69.6	36.7	47.6
✗	DRRQR	30%	18.3	27.4	48.5	29.0	52.3	55.2	70.4	33.2	48.1
✗	Grad	30%	17.2	11.9	50.3	26.8	50.8	54.6	70.8	47.5	50.1
✗	S-Wanda	30%	36.9	119.0	44.4	26.1	48.6	52.6	68.7	17.4	43.0
✓	L1	30%	18.1	12.8	50.0	27.0	49.3	52.9	70.0	45.9	49.2
✓	Rand	30%	17.4	12.0	50.4	26.9	49.6	53.9	70.3	46.6	49.6
✓	DRRQR	30%	16.8	10.5	51.1	27.4	50.0	53.9	70.0	50.2	50.4
✓	Grad	30%	16.9	10.1	51.3	26.5	50.4	54.8	70.6	51.1	50.8
✓	S-Wanda	30%	18.0	13.0	50.5	27.0	49.2	54.0	70.3	45.4	49.4
Baseline	–	0%	16.7	11.9	51.3	26.1	50.6	53.3	70.5	48.4	50.0

Table 11. Zero-shot performance of Gated DeltaNet 370M models, evaluated using the *lm-eval-harness* (Gao et al., 2024), given different compression ratios. Pre- and post RFT.

RFT	Method	Compr.	Wiki. ppl ↓	LMB. ppl ↓	ARC-e acc_n ↑	ARC-c acc_n ↑	Hella. acc_n ↑	Wino. acc ↑	PIQA acc_n ↑	LMB. acc ↑	Avg ↑
✗	L1	75%	116.4	1399.7	36.8	27.6	34.7	50.3	59.7	8.5	36.3
✗	Rand	75%	135.3	1078.1	41.5	26.5	34.4	51.2	60.4	11.2	37.5
✗	DRRQR	75%	45.9	97.8	49.7	27.8	38.4	50.1	63.7	23.8	42.3
✗	Grad	75%	<u>79.6</u>	<u>215.6</u>	41.5	27.9	37.4	50.0	62.9	20.1	40.0
✗	S-Wanda	75%	96.6	1205.5	37.2	26.5	35.5	50.4	60.6	8.8	36.5
✓	L1	75%	32.2	60.0	49.6	27.4	38.2	49.3	64.6	25.2	42.4
✓	Rand	75%	33.5	70.9	49.5	26.4	37.9	51.9	65.0	22.5	42.2
✓	DRRQR	75%	31.4	<u>53.5</u>	50.8	27.1	38.5	49.9	65.3	26.3	<u>43.0</u>
✓	Grad	75%	31.4	49.1	50.3	27.4	38.5	50.6	65.8	27.1	43.3
✓	S-Wanda	75%	<u>32.1</u>	58.2	50.0	27.0	38.0	49.3	64.5	25.6	42.4
✗	L1	50%	41.8	156.6	45.6	28.3	38.8	47.8	64.0	17.9	40.4
✗	Rand	50%	35.5	50.7	47.1	27.0	39.1	53.1	64.9	29.4	43.4
✗	DRRQR	50%	31.6	<u>39.4</u>	49.8	27.9	39.9	49.5	65.2	31.5	44.0
✗	Grad	50%	<u>33.3</u>	39.2	48.2	27.6	40.0	49.2	65.8	31.8	<u>43.8</u>
✗	S-Wanda	50%	40.0	141.5	45.5	28.7	38.9	49.6	64.0	18.9	40.9
✓	L1	50%	29.2	44.6	50.2	27.8	39.0	49.6	65.3	29.0	43.5
✓	Rand	50%	29.3	46.5	50.3	26.6	38.9	51.9	66.1	28.2	43.6
✓	DRRQR	50%	28.7	<u>40.6</u>	50.9	27.5	39.2	50.4	65.3	29.8	43.8
✓	Grad	50%	28.7	39.4	50.3	27.4	39.0	50.6	65.7	29.6	<u>43.7</u>
✓	S-Wanda	50%	29.2	44.6	50.3	27.3	39.1	50.2	65.0	29.0	43.5
✗	L1	40%	36.9	96.4	46.1	28.3	38.7	49.0	65.0	21.5	41.4
✗	Rand	40%	32.2	42.2	48.8	27.3	39.2	53.0	65.3	30.5	44.0
✗	DRRQR	40%	30.1	<u>38.3</u>	50.5	28.0	40.0	49.6	65.4	31.7	<u>44.2</u>
✗	Grad	40%	<u>30.7</u>	34.6	49.5	27.5	40.2	50.4	65.8	33.0	44.4
✗	S-Wanda	40%	35.9	95.8	46.7	28.0	39.2	50.2	64.1	22.1	41.7
✓	L1	40%	28.6	40.6	50.8	28.2	39.1	50.1	65.4	30.8	44.0
✓	Rand	40%	28.6	43.1	50.7	26.5	38.9	50.9	65.9	29.5	43.7
✓	DRRQR	40%	28.2	<u>39.5</u>	51.1	27.8	39.4	50.0	65.4	30.5	<u>44.0</u>
✓	Grad	40%	28.2	38.0	50.6	27.7	39.2	50.7	65.6	30.5	44.1
✓	S-Wanda	40%	38.5	40.6	50.9	27.8	38.8	49.6	65.2	30.8	43.9
✗	L1	30%	33.9	65.1	47.7	28.2	39.4	49.3	64.9	25.1	42.4
✗	Rand	30%	<u>29.9</u>	38.4	48.9	26.5	39.6	51.3	65.2	31.3	43.8
✗	DRRQR	30%	29.0	<u>36.6</u>	51.1	28.2	39.9	50.4	65.3	32.4	44.5
✗	Grad	30%	29.0	32.4	50.6	27.0	40.2	50.4	64.7	33.7	<u>44.4</u>
✗	S-Wanda	30%	33.2	66.5	47.4	27.7	39.5	50.0	65.2	25.3	42.5
✓	L1	30%	28.1	38.5	50.6	27.9	39.1	49.9	65.7	31.1	44.1
✓	Rand	30%	28.2	40.9	50.8	27.0	39.3	50.5	65.4	29.7	43.8
✓	DRRQR	30%	27.8	<u>38.0</u>	51.2	27.9	39.4	50.0	65.5	31.4	<u>44.2</u>
✓	Grad	30%	27.8	35.8	51.3	27.7	39.4	50.6	65.5	31.7	44.4
✓	S-Wanda	30%	28.0	38.8	50.5	28.0	39.1	49.0	65.3	30.7	43.8
Baseline	–	0%	28.8	35.9	51.5	28.2	39.6	50.4	65.5	31.5	44.4

Table 12. Zero-shot performance of Gated DeltaNet 1.3B models, evaluated using the *lm-eval-harness* (Gao et al., 2024), given different compression ratios. Pre- and post RFT.

RFT	Method	Compr.	Wiki. ppl ↓	LMB. ppl ↓	ARC-e acc_n ↑	ARC-c acc_n ↑	Hella. acc_n ↑	Wino. acc ↑	PIQA acc_n ↑	LMB. acc ↑	Avg ↑
✗	L1	75%	68.8	279.5	54.4	32.8	47.2	55.4	66.2	15.9	45.3
✗	Rand	75%	32.8	37.8	56.0	34.3	51.8	54.5	70.2	30.8	49.6
✗	DRRQR	75%	<u>22.5</u>	<u>23.6</u>	62.6	36.5	55.7	59.8	72.1	37.0	<u>54.0</u>
✗	Grad	75%	22.3	17.7	64.0	38.3	57.1	60.2	71.4	42.5	55.6
✗	S-Wanda	75%	30.6	77.0	59.7	36.3	54.3	58.9	69.9	24.6	50.6
✓	L1	75%	18.6	16.8	66.1	37.8	57.0	58.0	72.4	40.7	55.3
✓	Rand	75%	19.3	18.1	64.7	36.5	56.6	57.8	72.5	39.5	54.6
✓	DRRQR	75%	<u>17.9</u>	<u>14.7</u>	64.0	37.8	58.4	61.1	73.1	43.1	<u>56.2</u>
✓	Grad	75%	17.8	12.5	65.1	37.5	58.4	60.9	72.9	45.8	56.8
✓	S-Wanda	75%	18.2	15.1	63.9	37.7	57.5	59.0	72.6	41.7	55.4
✗	L1	50%	26.5	34.0	64.8	36.5	56.3	58.2	71.6	32.3	53.3
✗	Rand	50%	18.8	14.4	65.5	38.3	58.8	59.7	73.2	43.7	56.5
✗	DRRQR	50%	17.3	<u>14.2</u>	66.2	39.2	59.9	62.5	73.1	44.0	<u>57.5</u>
✗	Grad	50%	<u>17.4</u>	10.1	65.9	39.8	60.5	61.2	72.7	51.3	58.6
✗	S-Wanda	50%	21.9	24.1	65.1	38.5	58.7	60.0	72.1	36.1	55.1
✓	L1	50%	16.8	13.0	66.0	39.2	59.2	59.8	73.6	45.3	57.2
✓	Rand	50%	16.9	<u>11.5</u>	66.6	38.9	58.8	61.2	73.6	47.8	57.8
✓	DRRQR	50%	16.3	12.0	66.8	39.4	59.4	61.1	73.7	47.4	<u>58.0</u>
✓	Grad	50%	<u>16.4</u>	10.5	65.7	39.3	59.6	61.1	73.9	49.9	58.3
✓	S-Wanda	50%	16.6	11.7	66.6	39.2	59.4	60.5	73.8	47.3	57.8
✗	L1	40%	23.7	25.3	64.3	38.5	57.8	58.6	71.7	36.1	54.5
✗	Rand	40%	<u>18.3</u>	<u>11.0</u>	65.7	39.3	59.7	60.5	73.9	49.7	58.1
✗	DRRQR	40%	16.7	11.9	67.2	39.4	60.5	60.9	73.5	47.8	<u>58.2</u>
✗	Grad	40%	16.7	9.4	67.8	40.5	60.6	62.3	73.5	52.6	59.6
✗	S-Wanda	40%	20.7	21.6	65.4	39.6	59.5	60.3	72.4	37.4	55.8
✓	L1	40%	16.5	11.9	67.2	38.8	59.6	59.8	74.0	47.5	57.8
✓	Rand	40%	16.5	<u>10.7</u>	66.4	39.2	59.6	61.3	73.8	49.5	58.3
✓	DRRQR	40%	16.1	11.0	67.2	40.0	59.8	61.3	73.9	49.8	58.7
✓	Grad	40%	16.1	10.1	66.7	39.4	59.9	61.2	74.2	50.5	<u>58.6</u>
✓	S-Wanda	40%	16.4	11.5	66.8	39.5	59.9	60.8	74.2	47.7	58.1
✗	L1	30%	22.2	24.3	64.5	38.1	58.4	61.0	71.9	35.4	54.9
✗	Rand	30%	<u>16.7</u>	<u>11.4</u>	65.2	39.2	60.2	60.2	73.9	48.7	57.9
✗	DRRQR	30%	16.3	11.6	67.0	39.7	60.5	61.0	73.7	47.5	<u>58.2</u>
✗	Grad	30%	16.3	9.2	68.5	40.4	60.7	62.4	73.7	52.8	59.7
✗	S-Wanda	30%	19.8	18.4	65.5	39.8	60.1	61.5	73.1	39.7	56.6
✓	L1	30%	16.3	11.3	67.5	39.2	59.7	61.2	74.1	48.3	58.3
✓	Rand	30%	<u>16.1</u>	<u>10.2</u>	66.5	39.6	59.8	61.6	74.4	50.4	58.7
✓	DRRQR	30%	15.9	10.7	67.3	39.9	59.9	61.8	74.3	49.7	<u>58.8</u>
✓	Grad	30%	15.9	9.9	66.9	40.4	60.0	61.6	74.4	50.9	59.0
✓	S-Wanda	30%	16.1	11.0	67.6	40.3	60.0	60.5	74.0	49.0	58.6
Baseline	–	0%	16.8	9.7	67.7	41.0	60.1	62.2	74.0	51.5	59.4

Table 13. Accuracy of RFT’ed DeltaNet 370M on recall-intensive retrieval tasks with input truncated to $2K$ tokens, given different compression ratios. Computed using *prefix-linear-attention* (Arora et al., 2024).

Method	Compr.	Drop cont. \uparrow	FDA cont. \uparrow	NQ cont. \uparrow	SQuAD cont. \uparrow	SWDE cont. \uparrow	Triv. cont. \uparrow	Avg
L1	75%	11.6	1.3	9.1	15.9	6.4	37.7	13.7
Rand	75%	9.6	1.3	9.2	13.8	6.5	31.9	12.1
DRRQR	75%	14.4	2.3	10.7	18.5	7.1	39.6	<u>15.4</u>
Grad	75%	14.0	2.3	10.5	18.5	7.5	40.5	15.5
S-Wanda	75%	12.6	1.5	9.6	15.2	6.6	39.0	14.1
L1	50%	13.2	2.2	12.4	18.3	8.0	40.7	15.8
Rand	50%	14.5	3.2	11.8	18.6	7.9	40.8	16.1
DRRQR	50%	15.1	4.5	13.1	21.7	9.7	43.0	17.8
Grad	50%	15.1	5.1	13.1	21.5	9.2	42.9	<u>17.8</u>
S-Wanda	50%	13.1	2.6	11.8	18.7	7.1	40.1	15.6
L1	40%	13.3	2.8	12.3	18.6	8.5	40.6	16.0
Rand	40%	13.6	4.1	12.9	20.3	9.0	42.5	17.1
DRRQR	40%	15.8	6.0	14.1	22.3	10.2	44.0	18.7
Grad	40%	15.4	6.9	14.2	22.7	9.7	43.2	<u>18.7</u>
S-Wanda	40%	13.7	3.5	12.2	19.7	7.9	40.7	16.3
L1	30%	14.1	3.3	12.8	19.6	8.7	40.7	16.5
Rand	30%	14.8	4.5	12.5	21.7	9.2	42.0	17.4
DRRQR	30%	15.6	8.3	14.1	23.2	10.4	43.7	<u>19.2</u>
Grad	30%	15.1	8.6	14.1	23.8	10.5	43.4	19.3
S-Wanda	30%	14.6	4.3	12.5	20.7	8.3	41.8	17.0
–	0%	15.2	13.1	15.0	24.9	13.0	43.5	20.8

Table 14. Accuracy of RFT’ed DeltaNet 1.3B on recall-intensive retrieval tasks with input truncated to $2K$ tokens, given different compression ratios. Computed using *prefix-linear-attention* (Arora et al., 2024).

Method	Compr.	Drop cont. \uparrow	FDA cont. \uparrow	NQ cont. \uparrow	SQuAD cont. \uparrow	SWDE cont. \uparrow	Triv. cont. \uparrow	Avg
L1	75%	18.5	7.0	19.1	21.2	17.3	48.2	21.9
Rand	75%	17.3	7.1	17.3	22.1	15.2	46.6	20.9
DRRQR	75%	19.1	9.2	17.8	22.3	17.7	48.2	22.4
Grad	75%	18.9	15.6	20.3	26.0	20.9	51.4	25.5
S-Wanda	75%	17.4	7.7	19.1	21.8	17.3	49.9	22.2
L1	50%	20.7	23.1	21.6	27.3	29.0	53.0	29.1
Rand	50%	19.6	30.1	24.1	29.4	26.6	52.0	30.3
DRRQR	50%	20.0	31.5	23.3	28.7	29.2	53.6	<u>31.1</u>
Grad	50%	19.6	38.6	25.2	30.4	32.2	53.6	33.3
S-Wanda	50%	20.0	21.4	21.8	27.0	29.3	53.5	28.9
L1	40%	19.1	29.9	22.9	27.4	32.2	53.3	30.8
Rand	40%	21.1	32.9	24.8	30.0	31.7	52.8	32.2
DRRQR	40%	19.8	38.0	23.4	29.8	33.2	53.6	<u>33.0</u>
Grad	40%	20.3	44.6	25.7	31.1	35.6	54.4	35.3
S-Wanda	40%	19.8	29.5	23.2	27.4	32.2	53.6	31.0
L1	30%	21.5	34.2	24.9	28.4	31.6	53.9	32.4
Rand	30%	21.5	38.2	25.5	30.9	35.2	54.0	34.2
DRRQR	30%	20.6	41.7	24.9	30.5	34.9	53.8	<u>34.4</u>
Grad	30%	20.6	44.4	26.4	31.7	37.9	55.3	36.1
S-Wanda	30%	22.2	32.5	24.5	29.3	33.9	54.3	32.8
–	0%	21.0	57.8	27.2	34.6	42.8	57.5	40.1

Table 15. Accuracy of RFT’ed Gated DeltaNet 370M on recall-intensive retrieval tasks with input truncated to $2K$ tokens, given different compression ratios. Computed using *prefix-linear-attention* (Arora et al., 2024).

Method	Compr.	Drop cont. \uparrow	FDA cont. \uparrow	NQ cont. \uparrow	SQuAD cont. \uparrow	SWDE cont. \uparrow	Triv. cont. \uparrow	Avg
L1	75%	13.9	2.2	10.0	18.2	5.3	36.9	14.4
Rand	75%	13.8	2.2	10.2	17.6	4.8	37.1	14.3
DRRQR	75%	13.7	1.9	10.3	18.7	5.5	40.6	<u>15.1</u>
Grad	75%	14.1	2.3	10.3	19.4	5.3	40.0	15.2
S-Wanda	75%	15.1	2.2	10.3	18.0	5.2	38.0	14.8
L1	50%	16.1	5.8	12.5	22.8	9.5	41.7	18.1
Rand	50%	14.8	6.8	13.3	22.6	8.9	42.7	18.2
DRRQR	50%	16.1	4.6	13.0	23.4	10.4	42.6	<u>18.3</u>
Grad	50%	16.6	6.3	13.8	23.1	9.4	45.1	19.0
S-Wanda	50%	16.9	6.5	12.6	22.8	8.5	42.1	18.2
L1	40%	16.9	8.9	13.6	23.8	11.5	42.9	19.6
Rand	40%	16.4	10.7	13.9	24.2	10.7	42.8	19.8
DRRQR	40%	16.5	6.0	13.6	23.8	11.6	43.7	19.2
Grad	40%	18.2	8.1	14.1	24.1	11.9	45.2	20.3
S-Wanda	40%	17.1	9.9	14.1	23.9	10.6	43.5	<u>19.8</u>
L1	30%	18.5	11.1	14.0	24.6	13.1	43.7	20.8
Rand	30%	16.4	13.0	14.7	25.0	12.6	43.4	20.8
DRRQR	30%	17.8	8.3	14.7	24.7	12.8	44.6	20.5
Grad	30%	18.4	9.6	15.1	25.2	12.8	45.6	21.1
S-Wanda	30%	19.2	9.4	14.6	25.1	12.6	44.1	20.8
–	0%	18.1	16.3	16.0	26.8	16.8	46.1	23.3

Table 16. Accuracy of RFT’ed Gated DeltaNet 1.3B on recall-intensive retrieval tasks with input truncated to $2K$ tokens, given different compression ratios. Computed using *prefix-linear-attention* (Arora et al., 2024).

Method	Compr.	Drop cont. \uparrow	FDA cont. \uparrow	NQ cont. \uparrow	SQuAD cont. \uparrow	SWDE cont. \uparrow	Triv. cont. \uparrow	Avg
L1	75%	18.4	13.4	20.5	29.1	15.8	56.8	25.7
Rand	75%	19.2	11.2	18.0	28.0	14.1	52.8	23.9
DRRQR	75%	17.9	18.7	19.9	28.7	15.0	56.1	26.1
Grad	75%	17.8	17.3	21.1	29.1	17.2	58.7	26.9
S-Wanda	75%	18.9	15.6	20.8	28.5	16.0	57.6	<u>26.2</u>
L1	50%	22.8	28.9	24.3	34.9	25.4	60.9	32.9
Rand	50%	20.3	31.1	23.0	33.3	25.2	59.8	32.1
DRRQR	50%	20.5	32.1	23.5	33.6	26.5	61.6	33.0
Grad	50%	20.8	36.6	24.5	33.8	28.4	61.7	34.3
S-Wanda	50%	21.3	32.8	24.2	33.4	25.4	62.1	<u>33.2</u>
L1	40%	22.4	33.1	25.9	34.7	29.6	62.1	34.6
Rand	40%	22.2	39.5	24.0	34.7	26.0	61.2	34.6
DRRQR	40%	21.5	39.1	24.6	34.8	29.2	61.1	<u>35.0</u>
Grad	40%	21.7	39.8	25.1	34.7	31.1	62.7	35.8
S-Wanda	40%	22.1	39.1	24.1	34.6	25.1	61.5	34.4
L1	30%	20.9	37.2	26.0	35.4	30.5	62.4	35.4
Rand	30%	22.8	44.4	25.1	35.6	33.4	62.6	<u>37.3</u>
DRRQR	30%	21.6	42.4	25.2	35.4	32.2	61.9	36.5
Grad	30%	22.6	45.7	26.4	36.2	33.7	63.5	38.0
S-Wanda	30%	22.6	44.2	24.9	35.3	33.5	62.6	37.2
–	0%	22.1	53.7	27.0	37.0	37.5	64.5	40.3

H. More Plots

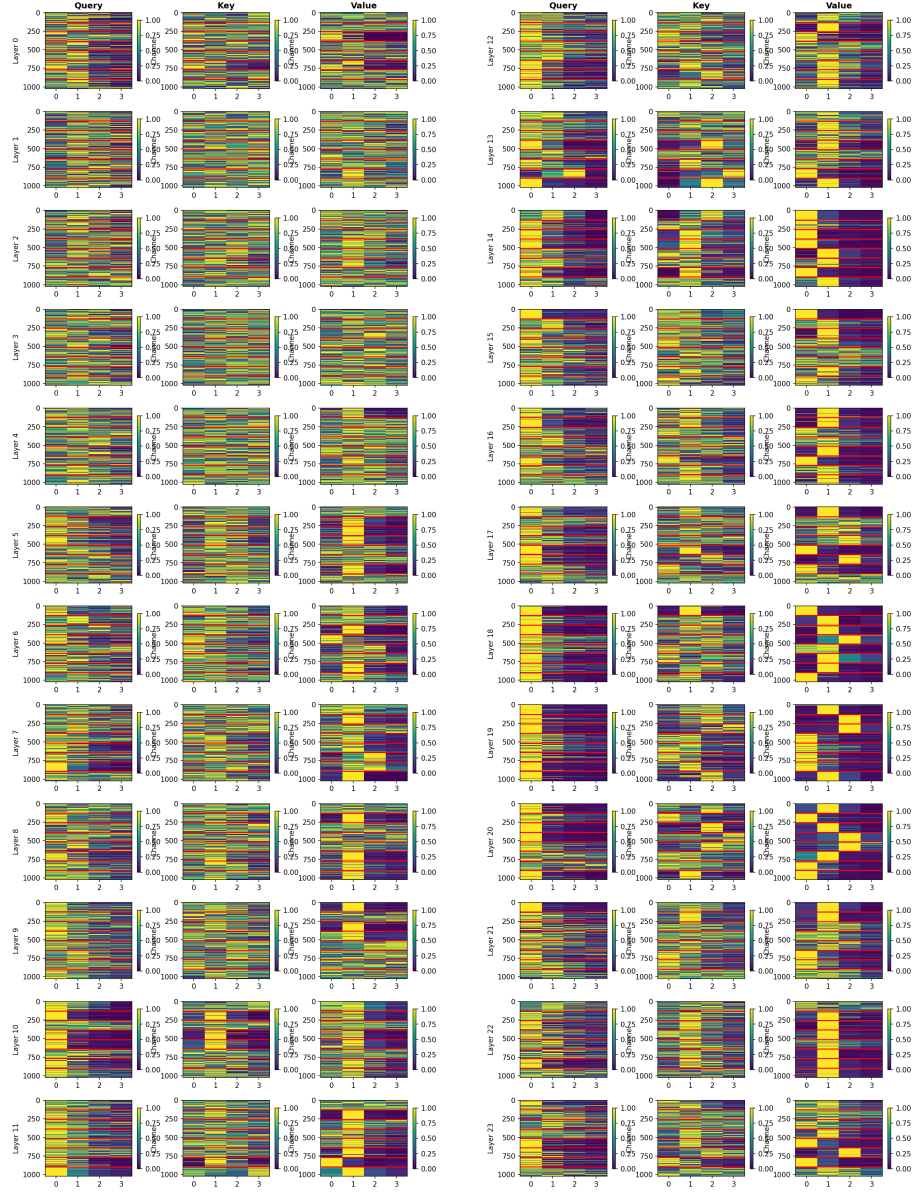


Figure 5. Convolution filters for queries, keys, and values of a standard DeltaNet 370M (non-shared). High similarity within heads (separated by red lines) suggests implicit sharing.

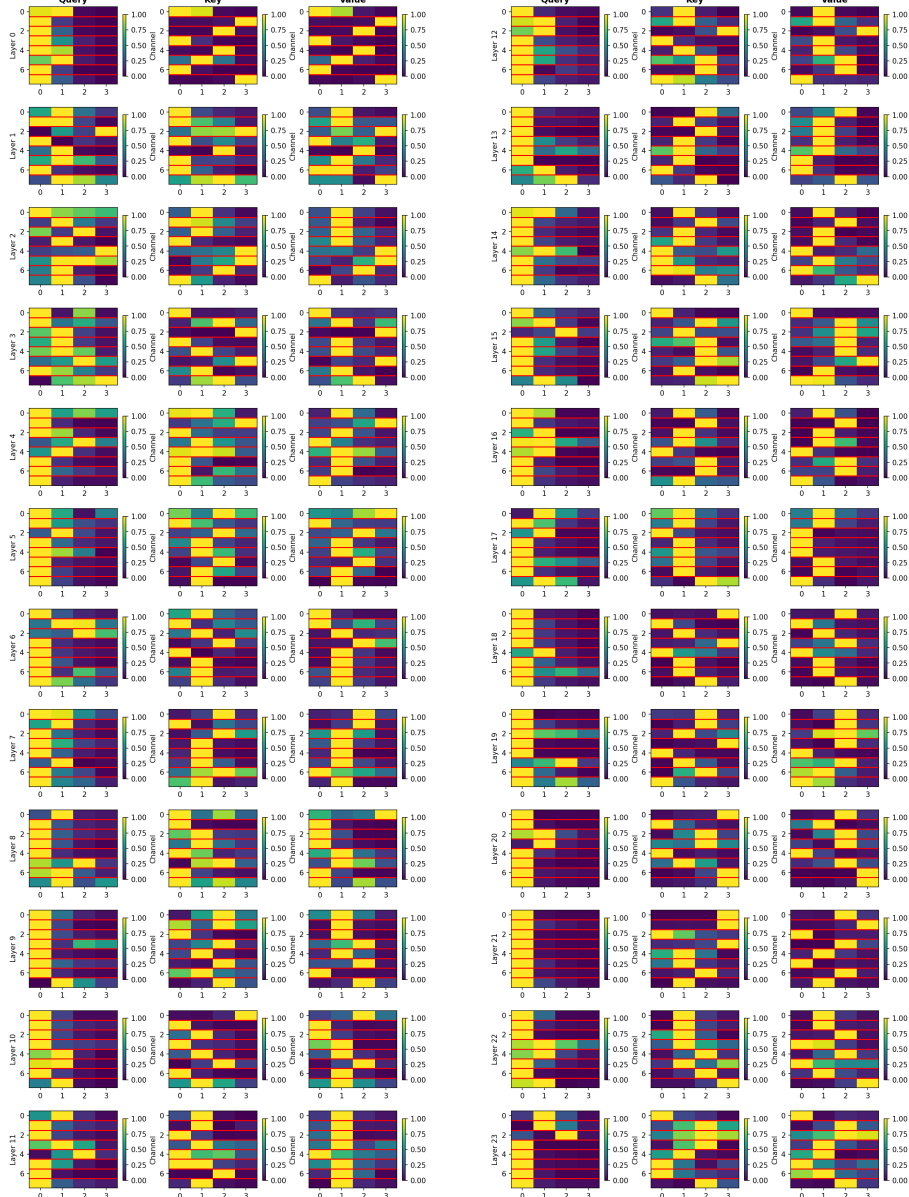


Figure 6. Convolution filters for DeltaNet 370M with explicitly shared convolutions. The model learns distinct patterns for Q, K, and V.